CASE FILE
COPY

RM L50I21

NACA RM L50I21

NACA

RESEARCH MEMORANDUM

DESCRIPTION AND INVESTIGATION OF A DYNAMIC MODEL OF THE XH-17 TWO-BLADE JET-DRIVEN HELICOPTER

By George W. Brooks and Maurice A. Sylvester

Langley Aeronautical Laboratory
Langley Field, Va.

NATIONAL ADVISORY COMMITTEE
FOR AERONAUTICS

WASHINGTON
March 14, 1951

NATIONAL ADVISORY COMMITTEE FOR AERONAUTICS

RESEARCH MEMORANDUM

DESCRIPTION AND INVESTIGATION OF A DYNAMIC MODEL OF THE XH-17 TWO-BLADE JET-DRIVEN HELICOPTER

By George W. Brooks and Maurice A. Sylvester

SUMMARY

A description and results of an investigation of a $\frac{1}{10}$-scale dynamic model of the XH-17 two-blade, jet-powered helicopter is presented. Tests were made with a configuration which corresponded to the configuration of the prototype and with a configuration which had several modifications. These modifications included varying the size of blade counterweights, changing the control stiffness and chordwise bending stiffness of the blades, and varying the pylon and undercarriage damping and spring constants for different model gross-weight conditions.

In flutter tests of the model, rotor-blade flutter of the classical bending-torsion type was encountered at rotor speeds corresponding to full-scale tip speeds near the overspeed limit of 800 feet per second. When the natural frequencies of the blades in first torsion were adjusted so that the frequency in the cyclic mode was approximately equal to the frequency in the collective mode, it was observed that the blades would flutter in either the cyclic or collective mode, depending on whether the model was externally vibrated. The test results showed that the flutter speed could be raised either by placing weights in the outboard counterweight boxes ahead of the leading edges of the blades or by increasing the natural frequencies of the blades in first torsion. Flutter tests made with the model rotor mounted on a rigid pylon showed the design counterweights to be more effective in eliminating pitch divergence than in eliminating flutter.

No unstable ground vibrations were observed during any of the model tests. These tests included runs for which most of the pylon damping and spring constants were varied in the order of from 3/4 to 2 times the design value.

INTRODUCTION

The development of helicopters has accelerated rapidly in recent times both from an aerodynamic and structural standpoint, but there still exist many vibrations problems common to most helicopters. In an effort to obtain a clearer understanding of some of these problems, the National Advisory Committee for Aeronautics has undertaken some analytical and experimental work on vibration and flutter aspects of helicopters. As a part of the investigation it was considered expedient to perform some of the work for a specific model of a full-scale prototype and to divide this work into two phases: a first phase dealing more specifically with parameters that correspond to values of the full-scale helicopter, and a second and more general phase which involves a variation of the model parameters. The present paper deals with the first phase of this work and relates to the XH-17 helicopter.

The XH-17 helicopter is a large helicopter having many unconventional features, among which are the following:

(1) The helicopter has a jet-powered rotor which is 130 feet in diameter and composed of two ducted blades. Each blade is equipped with four jets located near the blade tip. Compressed air is supplied to the blade-tip jets at an absolute pressure of approximately $2\frac{1}{2}$ atmospheres by two axial-flow compressors located in the fuselage. Additional thrust is obtained by burning fuel in these jets.

(2) The blades are connected to the hub by two laminated blade-retention straps which transfer the centrifugal forces into the hub and permit the blades individual freedom in the flapping plane. The lag motion of the blades is effectively eliminated by the blade centrifugal forces.

(3) Each blade is equipped with two counterweights which are used to adjust the blade center-of-gravity distribution and flutter characteristics. The counterweights are located ahead of the blade leading edge at radial position of $\frac{r}{R} = 0.13$ and 0.85, respectively.

(4) The pylon is attached to the fuselage in a manner which permits it to float, that is, to translate relative to the fuselage with the motion of a springloaded parallelogram-linkage system. The spring constant and natural frequency of the pylon motion relative to the fuselage are reduced as the rotor thrust is increased.

These unconventional features are believed to be of general interest to designers of large helicopters and warranted the study of a dynamic model. It was deemed advisable to use a scaled dynamic model because the experimental results could serve as a useful guide in the analytical studies, particularly in the selection of the important vibration modes.

This paper presents the design scale factors and discusses the construction and initial tests of the model. The model was chosen to be a $\frac{1}{10}$-scale model. Tables and figures are included to show the significant model parameters and design features, and results of the ground-vibrations tests and flutter tests are presented. In addition, the paper presents the general characteristics of a 3-per-revolution antisymmetric blade-bending oscillation recorded during the tests.

APPARATUS AND METHODS

Model Scale Factors

Before giving a detailed description of the model, a summary of the model scale factors is presented. One important consideration in the determination of these scale factors is the Reynolds number effect. Strictly speaking, for complete similarity, the Reynolds number of the model and prototype should be the same. In order to meet other scale-factor requirements, however, the condition of Reynolds number similarity could not be met. Even so, it was believed that the Reynolds number effects could be minimized if the model scale factors were chosen such that the overspeed Reynolds number of the model blade tips was of the order of one million or more. To meet this consideration and to obtain sufficient detail in the model, a scale factor of 1/10 for length was found suitable. For classical flutter similarity, κ for the model and prototype must be the same, where κ (see references 1 and 2) is given by the equation $\kappa = \frac{\pi\rho b}{M}$ in which:

ρ air density, slugs per cubic foot

b blade half chord, feet

M blade spanwise mass distribution, slugs per foot

From this relation and the scale factor for length, the scale factor for weight was determined to be 1/1000. Coleman has shown in references 3 and 4 that in the extreme case where the inertia forces and air forces are dominant in comparison with the elastic forces, a flutter phenomenon characterized by a low flutter frequency may be encountered on helicopter rotor blades. Since this low-frequency type of helicopter-rotor-blade flutter is dependent on the blade coning and pitch angles, the model and full-scale helicopter in the hovering condition should be operated at similar section lift coefficients. From this consideration and the scale factors for length and weight, the scale factor for rotor rotational frequency is fixed at $\sqrt{10}$, which is also the scale factor for all other characteristic model frequencies.

For these scale factors and atmospheric test conditions, the condition of Mach number similarity cannot be met. The overspeed tip Mach number obtained on the model during the tests was approximately 0.22, whereas the corresponding overspeed tip Mach number for the prototype is approximately 0.70. These values are based on a prototype tip speed of 800 feet per second. This difference in model and full-scale Mach numbers should be kept in mind when the model test results are used to predict full-scale phenomena.

When the scale factors for length, mass, and frequency have been obtained, all other scale factors may be obtained either from the equations of motion for flutter and ground vibrations, or by the use of dimensional analysis. The scale factors of general interest are:

Mass	$1/1000$
Length	$1/10$
Length ratios (that is, c.g. location in percent of blade chord)	1
Frequency	$\sqrt{10}$
Time	$1/\sqrt{10}$
Velocity	$1/\sqrt{10}$
Air density	1
Mass moment of inertia	$1/10^5$
Bending stiffness (EI)	$1/10^5$
Torsional stiffness (GJ)	$1/10^5$
Linear spring constant	$1/10^2$
Viscous damping constant	$\frac{1}{10^2\sqrt{10}}$

Summary of Model and Full-Scale Parameters

The pertinent full-scale helicopter parameters were supplied by the Hughes Aircraft Company and were used as a guide in designing the model. A summary of some of the model and full-scale parameters is presented in tables I, II, and III, and in figures 1 and 2.

Table I presents a comparison between the model and full-scale spanwise distribution of κ as well as the average values. Table II presents a comparison of the rotor-blade natural frequencies during the three series of model flutter tests. The frequencies are given for the blades resting on the droop stops and for the blades supported off the droop stops by elastic chords located at blade station 65.5. The model values are expressed in terms of the corresponding full-scale values by use of the indicated scale factor. Table III compares the model parameters used during the ground-vibrations tests with full-scale values for two different gross-weight conditions. Again the model values are converted to full-scale values by use of indicated scale factors.

Figures 1 and 2 present a comparison between the model and full-scale spanwise distributions of the blade mass and chordwise center-of-gravity location.

Model Description

Since the investigation is concerned only with the dynamic properties of the helicopter it was not necessary to construct an exact scale model of precise detail, but rather a dynamic model which would contain the major degrees of freedom and design features of the full-scale helicopter. In an effort to obtain results of a more general nature, provisions were made for varying the model parameters so as to obtain tests results over a wide range of model operating conditions. A general description of the model follows and is given with the aid of general view and close-up photographs (figs. 3 to 9) and with the aid of schematic diagrams (figs. 10 to 13).

Model power supply.- The XH-17 dynamic model is powered by compressed air, drawn from a 2-inch supply main at a static pressure of 105 pounds per square inch absolute. The air supply to the rotor is controlled by a gate valve, from which it passes upward through a series of small flexible tubes to the pylon manifold, (see figs. 3, 4, and 6) through the pylon and hub to the inboard-blade manifolds. From the inboard manifold, the air passes through two fabricated flexible tubes into the outboard manifold and through the jet nozzles. These jet nozzles are located four at each tip and are placed along the chord line perpendicular to the quarter-chord line. (See fig. 5.) The jet nozzles are a parabolic-convergence - straight-tail-pipe design with an inlet diameter of 0.75 inch, a throat diameter of 0.23 inch, and a tail-pipe length of 3 inches.

The tail rotor on the prototype is replaced by a jet nozzle similar to the rotor nozzles except that no tail pipe is used. The air is supplied from the supply main through a separate gate valve and hose system to the nozzle.

Rotor blades.- The rotor blades are shown in figures 3, 4, 5, and 10. The blades are of rectangular plan form, untwisted, and have a chord of 6.8 inches. The rotor has a diameter of 13 feet and a solidity of 0.055. The airfoil section is the NACA 23018. The blade spanwise weight distribution is given in figure 1 and the spanwise distribution of the chordwise center-of-gravity location is given in figure 2. The curves of figures 1 and 2 do not include the effects of the inboard counterweights which are shown on the figures as concentrated weights. The basic blade structure consists of a $\frac{1}{4}$-inch round spar of 24S0 aluminum alloy located along the quarter chord. Aluminum ribs are welded to the spar at intervals of 6.55 inches. Interspersed at equal intervals between

the metal ribs are three balsa ribs. Balsa stringers are placed along the leading and trailing edges to support the skin. The skin consists of $\frac{1}{32}$-inch balsa (6 lb/cu ft) glued to the ribs with the grain running spanwise and covered by linen fabric fastened to the balsa with dope. Since balsa is used on the model and since the ratio of the shear to tension modulus is considerably lower for balsa than the aluminum used on the prototype, the linen fabric is laid on the bias, with respect to the blade quarter-chord line, to bring the blade torsional rigidity up to the desired value. The aluminum spar (see fig. 5) structurally connects the inboard-transition manifold to the outboard-jet manifold. The compressed air is carried between the manifolds by two $\frac{7}{8}$-inch-diameter tubes which pass through the ribs and lie, one on each side of the metal spar. The air tubes are fabricated by wrapping linen tape around vinylite tubing and bonding with rubber cement. The tape, 4 inches in width, is first wrapped longitudinally (in cigarette fashion) to prevent lengthening and then spirally to prevent radial expansion. This type of construction was necessary to obtain a lightweight, flexible tube of high strength and durability.

The two inboard metal ribs are joined together at the top and bottom surfaces by welded aluminum-alloy plates. (See end rib plates in fig. 5.) Two cover plates are used to connect the flanged transition piece (inboard manifold) to the rib plates. The blade skin extends over the rib plates and is held between the rib plates and cover plates. Small lugs are attached to the leading and trailing edges of each metal rib so that additional weights may be added to change the chordwise center-of-gravity position if desired. An additional means of changing the chordwise center-of-gravity position is provided by varying the mass and chordwise location of the inboard and outboard counterweights. (See fig. 10.) The outboard counterweight box is a balsa-covered aluminum frame attached to the blade at $\frac{r}{R} = 0.85$. A section of the cover opens and allows access to a threaded steel rod upon which additional weight may be placed and adjusted. The inboard counterweight is simply a threaded aluminum-alloy rod containing an adjustable brass weight which extends forward of the leading edge in a plane 8° below the plane of the chord line and is attached at $\frac{r}{R} = 0.13$. The weight-distribution curves of figure 1 include the design values for the outboard counterweights. The model inboard counterweight as well as the full-scale inboard counterweight, pitch bearing housing and droop stop are shown as concentrated weights.

Rotor hub and suspension system.- The rotor hub is shown in figures 6, 7, 10, and 12. The hub T-spinner is cast magnesium which is machined to fit two lightweight helicopter type of ball bearings which are located one each at the top and bottom of the spinner housing. The thrust load is transferred from the spinner, through the bearings to the spinner housing, through the connecting arms to the bottom bay of

the suspension system, up the vertical links to the top bay and into the fuselage. (See fig. 12.) The rotor blades are permitted to pitch by use of bearings at the inboard ends. (See bearing housing in fig. 10.) These bearing housings are restrained from rotating by two cantilever arms but are allowed to extend spanwise by means of sliding pins attached to the free ends of the cantilevers. Flexible bronze bellows are used to provide a flexible air passage between the T-spinner and the bearing housings. The centrifugal loads are transmitted to the T-spinner by flexible steel straps.

As illustrated by the sketches of figure 11, the suspension system is essentially a parallelogram, the bottom bay of which is rigidly attached to the spinner housing and the top bay rigidly attached to the fuselage. A, B, C, D, E, F, G, and H are universal joints. The bottom bay, E, F, G, H, is restrained in translation relative to the top bay, A, B, C, D, by four torsion-spring assemblies similar to the detail of link GH. These torsion springs provide a relative spring constant between the pylon and fuselage of 24.28 pounds per inch in any horizontal direction. This type of suspension system prevents rotation of the bottom bay relative to the top bay. The top bay is also connected to the pylon by four viscous dampers, situated so as to dampen the relative motion between the pylon and fuselage equally in all directions.

Fuselage.- The fuselage is constructed of welded aluminum tubing, (see figs. 3, 4, and 6). In scaling the fuselage, only the over-all dimensions were scaled and no attempt was made to scale the structural rigidity or stress distribution of the prototype. Ballast weights may be added to the fuselage to obtain the desired weight conditions, center-of-gravity locations, and fuselage moments of inertia. (See figs. 3, 8, and 9.) The tail jet is located at the tip of the tail boom.

Landing gear.- Figures 8 and 9 show the front and rear wheel-strut assemblies, respectively. As shown in figure 8, the front strut is canted forward 12°. Due to the fact that this forward cant produced a considerable bending moment in the strut and caused the struts to bind under high gross weight conditions, these struts were later adjusted to a vertical position as shown in figure 3. The ballast weights shown are those mentioned in a previous paragraph. The strut assembly consists of an aluminum-alloy strut and damper, and two semicircular steel springs rigidly attached to the strut at each end. The dampers consist of two concentric cylindrical surfaces with a circumferential clearance of approximately 0.001 inch. The outer cylinder contains an oil groove, 1/16 inch deep and 1/4 inch wide (along the cylinder axis) cut around the inner circumference at the center of the cylinder to maintain constant lubrication. Fluids of various viscosities are used to vary the damping constant. The dampers, as shown in the figures, are covered with rubber sleeves to shield them from dust and other foreign matter. The spring constant of the strut assembly may be adjusted by clamps located around the circumference of the springs (faintly visible in fig. 3). The wheels and tires are standard model aircraft parts. The air pressure in the tires may be varied from 0 to 10 pounds per square inch with a resulting

variation in the tire spring and damping constants. To simulate the brakes-on condition the rear wheels may be locked by tightening the axle nut.

Control system.- The swash plate-control assembly is shown in figures 7 and 13. The swash plate is mounted on a sleeve (see also fig. 12) which is moved vertically on the spinner housing by a double-acting hydraulic cylinder. Figure 7 shows the sleeve in the extended position, that is, the location for maximum-blade collective pitch. Two other double-acting hydraulic cylinders are mounted on the sliding sleeve, located 90° apart around the sleeve, and provide for cyclic-pitch variation by actuating the gimbal rings of the swash plate. The three model control cylinders are actuated by master control cylinders located at the control station. The model and master cylinders are connected by flexible tubing supplied with hydraulic fluid under pressure. As a safety precaution, guy cables are attached to the upper-fuselage bay and are rigged to permit the model to be pulled to the floor.

Instrumentation.- The instrumentation of the model is accomplished by the use of accelerometers and electrical-resistance strain gages. Both blades are equipped with strain gages at the inboard blade sections $\frac{r}{R} = 0.36$ to indicate blade bending and torsion. Strain gages are also located on the cyclic-pitch coupling arm to indicate cyclic-blade root-pitching motion of the rotor blades and on cantilever springs to indicate the motion of the pylon relative to the fuselage. Five accelerometers are located on the fuselage to indicate motion in any of its six degrees of freedom. The instantaneous rotor speed in rpm is observed with the aid of an optical device consisting of a mirror and rotating prism. A measure of the exact rotor speed is also obtained on an oscillograph record by a one-per-revolution rotor speed timer.

Testing Technique

All the model tests were made indoors at zero forward velocity. The test results were recorded with an oscillograph; in addition, the ground-vibrations tests were photographed with 16-millimeter motion-picture cameras.

Some of the flutter tests were made with the model tethered to the floor by taut guy cables and with the wheel-strut assemblies replaced by flanged supports. (See fig. 4.) The pylon dampers were replaced by rigid links to eliminate the relative motion between the pylon and fuselage. This was done to insure that no unstable ground vibrations would occur during these tests. Furthermore, it was not believed that the flutter speed would be changed appreciably by tethering the model to the floor. Following these tests, ground-vibrations tests were made and

additional flutter tests were run with the model mounted on its tires and with all dampers installed. The only model restraints used during these flutter tests were the four safety cables attached to the upper bay of the fuselage which were used to hold the model near the floor. During some of these tests, the model was shaken vigorously in an effort to determine the effect of externally applied vibrations on the flutter characteristics. After these tests, the rotor was mounted on a rigid pylon with the rotor plane located 52 inches above the floor to determine the effect of the counterweights on flutter. During all of the flutter tests, the rotor speed was slowly increased until flutter was obtained, or in the absence of flutter, until 4/3 design speed was reached. This represents a model tip speed of 251 feet per second and corresponds to a prototype tip speed of 800 feet per second.

In the ground-vibrations tests, the model was completely assembled and the guy cables relaxed and used as safety restraints to keep the model from drifting while air-borne. (See fig. 3.) The blade-pitch control stiffness was increased sufficiently to eliminate the possibility of flutter during the ground-vibrations tests. The rotor speed was varied in increments of 40 rpm until the model became air-borne. Following each increment in speed, the model was rocked in both the pitching and rolling planes; the subsequent motion was observed and recorded.

RESULTS AND DISCUSSION

Flutter Tests

Three series of flutter tests were made on the model and one series with the model rotor mounted on a rigid pylon. These tests represented a wide range of operating conditions, particularly in the variation of the blade torsional frequencies and counterweight configurations. The blade frequencies for the model tests are presented in table II accompanied by sketches to identify the various bending modes. The "off stops" frequencies were obtained by supporting the blades with elastic cord of very low stiffness at station 65.5. The model frequencies have been converted to the corresponding full-scale values and presented along with the full-scale frequencies which represented that particular test condition. Although the control-system linkage for the tests made with the rotor mounted on the rigid pylon was identical to that used during the third series of model flutter tests, the natural frequencies of the rotor when mounted on the rigid pylon are increased approximately 25 percent. A summary of the flutter test results is presented in tables IV and V and a chart for conversion of model speeds and frequencies to the corresponding full-scale values is presented in figure 14. The only type of flutter encountered during the tests was the classical type of bending-torsion flutter. A description of and the results found in each of the four series of tests follows.

First series of flutter tests.- The first series of flutter tests was run with the pylon rigidly attached to the fuselage (that is, the dampers were replaced by rigid links) and with the fuselage fastened to the floor. (See fig. 4.) In these tests, flutter involving cyclic torsional motion and antisymmetric bending motion of the blades was encountered. (See table IV.) A portion of the oscillograph record of the flutter is shown in figure 15. The flutter speed was raised by placing weights in the outboard counterweight boxes ahead of the blade leading edges. As soon as flutter was observed, the power to the rotor was cut off; therefore, the duration of flutter as given in table IV may have been influenced accordingly.

Second series of flutter tests.- The second series of flutter tests was made with the model assembled in the same manner as for the first series of tests. The major difference in the model parameters during the first two series of flutter tests was the difference in the torsional frequencies of the blades. The torsional frequencies were varied by changing the blade control stiffness. The second series included runs at various pitch angles and counterweight configurations. These variations are shown in table IV. No flutter was encountered during any of these tests.

Third series of flutter tests.- The third series of flutter tests were made after the ground-vibration tests and with the model mounted on its landing gear and free to vibrate in all of its degrees of freedom; the only restraints were the four safety wires attached to the upper bay of the fuselage which were held in a relaxed position to allow the model to vibrate vertically or rock on the tires. In addition to the blade frequencies given in table II and the flutter test results given in table IV, some additional parameters are important for these tests. These are converted to the corresponding full-scale values and are listed as follows:

Weight of items suspended on the suspension system, pounds	18,080
Fuselage weight, pounds	23,730
Gross weight, pounds	41,810
Fuselage moment of inertia (rolling), slug-feet^2	30,500
Fuselage moment of inertia (pitching), slug-feet^2	43,200
Fuselage center-of-gravity location (below rotor plane), inches	137
Damping constants:	
Wheel-strut assembly (front), pound-seconds per foot	442
Wheel-strut assembly (rear), pound-seconds per foot	544
Pylon (minimum value), pound-seconds per foot	900
Spring constants:	
Wheel-strut assembly (front), pounds per inch	1610
Wheel-strut assembly (rear), pounds per inch	3080
Pylon (at zero thrust), pounds per inch	4600
First chordwise blade bending (on stops), radians per second	11.90

The third series of flutter tests were divided into two groups of three runs each and these tests were made with the inboard and outboard counterweights adjusted to the design values as given in figure 1.

During the first group of runs, the model restraints were held in a position to allow the tires to just clear the floor when the thrust equaled the gross weight. The rotor speed was slowly increased until flutter was obtained. In each case the flutter occurred in the symmetric or collective mode which caused the model to vibrate considerably in the vertical direction.

During the second group of flutter runs, the model was shaken vigorously by the safety cables as the rotor speed was increased. This shaking was done in an effort to study the effect of such vibrations on the flutter mode, flutter speed, and flutter frequency and to see whether it was possible to excite unstable ground vibrations and flutter simultaneously. Flutter was obtained during each run, but no unstable ground vibrations were observed. The flutter occurred in the antisymmetric or cyclic mode.

Although in these tests the initial collective pitch angle, measured from the angle of zero rotor thrust, was set at 0.5°, the rotor was developing approximately 50 pounds of thrust at speeds near the flutter speeds. This condition was attributed to the fact that the centrifugal forces acting on the blade-retention straps were sufficiently high to increase the collective pitch angles by overcoming the stiffness of the controls. If when flutter is first encountered the power is held constant, the flutter will not continue; but, instead, the increase in drag encountered during flutter is sufficient to slow the rotor down until flutter temporarily disappears. The rotor speed will then increase until flutter reappears and the cycle is repeated.

Flutter tests with rigid pylon.- These flutter tests were made with the model rotor mounted on a rigid pylon at a height of 52 inches above the floor. The purpose of these tests was to obtain a more qualitative evaluation of the effect of the various counterweight configurations. The blade pitch angle and control stiffness was identical to that used in the third series of flutter tests, however, the flutter mode was altered somewhat because the rotor hub was restrained from moving either laterally or vertically. In addition, the natural frequencies of the blades were increased approximately 25 percent because of the increased pylon rigidity. The results of these flutter tests are presented in table V. In each test the flutter occurred in the antisymmetric mode and there was a pronounced tendency for pitch divergence to precede flutter as the counterweights were progressively removed.

As a result of the aforementioned tests, it is concluded that the model will flutter in either the cyclic or collective mode if the natural torsional frequencies of the blades in these modes are similar. If the model is not externally excited, it will flutter in the collective mode; but if it is externally excited, it will flutter in the cyclic mode. These facts are borne out by the third series of flutter tests, even

though the torsional frequency in the collective mode was somewhat higher than in the cyclic mode. The flutter speed can be increased either by increasing the torsional frequencies of the blades or by placing weights in the outboard counterweight boxes ahead of the blade leading edges. As a result of the flutter tests made with the rotor mounted on a rigid pylon, it is concluded that the counterweights are more effective in preventing divergence than in preventing flutter; however, as shown in table V, the flutter speed is somewhat higher with the counterweights attached.

Ground-Vibrations Tests

Two series of ground-vibrations tests were conducted on the model. These tests followed the first two series of flutter tests. During these tests, the model was completely assembled as shown in figure 3. The test procedure consisted of raising the rotor speed in increments of 40 rpm until the model became air-borne. Following each increment in speed, the fuselage was rocked in both the pitching and rolling planes and the subsequent motion observed and recorded. This procedure was repeated for each collective pitch setting in an effort to excite possible instabilities but none were observed. The theory of ground vibrations of helicopter rotors is presented in references 5 to 7 and the reader is referred to these papers for a discussion of the significance of the various parameters involved.

First series of ground-vibrations tests.- For the first series of ground-vibrations tests, the model parameters were adjusted to values which were believed to minimize the occurrence of unstable ground vibrations; that is, low gross weight, high damping, and high spring constants. The runs were made at a blade pitch setting of approximately 4° and the model hovered at a rotor speed of 274 rpm.

The more significant model parameters for the first series of ground-vibrations tests are presented in table III. In order to minimize the possibility of unstable ground vibrations, the front and rear wheel-strut assemblies were adjusted to provide effective damping and spring constants higher than design conditions. The values of these constants were determined with the gross weight of the model supported on the tires. As the model tended to hover the tire spring constant reduced slightly; thereby, the effective spring constant of the wheel-strut assembly was reduced. The effective pylon damping was supplied by the pylon dampers, friction in the suspension system, and the four air-supply tubes attached to the pylon. The damping due to the pylon dampers and the air-supply tubes remained relatively constant with rotor thrust, whereas the friction damping varied considerably, being a minimum when the rotor thrust equaled the suspended weight of 18.08 pounds. The type of pylon suspension used (fig. 11) causes the effective horizontal spring constant of the pylon to decrease slightly with increase in thrust. The effective pylon spring

and damping constants are given in figure 16 as a function of thrust. Since a theoretical analysis by the Hughes Aircraft Company showed that the 2-per-revolution vibrations of the pylon induced by the rotor blades would be diminished by increasing the pylon spring constant above the design values, coil springs were installed on the pylon to increase the horizontal spring constant to 61 pounds per inch at zero rotor thrust with the suspended weight of 18.08 pounds supported on the suspension system. Because of instrumentation and the addition of mass to meet the inertial requirements of the fuselage, the minimum model weight corresponding to the minimum gross weight of the full-scale helicopter was not realized.

Runs were also made during the first series of ground-vibrations tests with the pylon dampers removed, the rear brakes both locked and unlocked, and all other parameters unchanged. No unstable ground vibrations were observed.

Second series of ground-vibrations tests.- The second series of ground-vibration tests were conducted in a similar manner except that the model parameters were adjusted, insofar as possible, to the values which would more likely produce unstable ground vibrations. The one exception is that the spring constants of the model landing gear are slightly higher than the full-scale values. These values were accepted because the configuration provided lower damping constants. Runs were made at pitch settings of approximately 3°, 5°, and 10°. The hovering rotor speeds at these pitch settings were 375, 320, and 245 rpm, respectively.

The significant model parameters for the second series of ground-vibration tests are contained in table III. The strut dampers and springs were locked in position for these tests, the resulting spring and damping constants of the undercarriage being attributed solely to the tires. The tire spring and damping constants were adjusted by reducing the air pressure of the tires to $2\frac{1}{2}$ pounds per square inch. The pylon dampers were removed along with two air-supply tubes to reduce the pylon damping to a minimum. (See fig. 16.) The resultant pylon damping was therefore supplied by the friction in the suspension system and the two remaining air-supply tubes. Light coil springs were installed on the pylon to increase the horizontal spring constant to 46 pounds per inch at zero rotor thrust with the suspended weight of 17.82 pounds per inch supported on the suspension system.

Although only two series of ground-vibration tests are reported herein, a much greater range of operating conditions was actually covered; that is, several intermediate runs were made while approaching the conditions for the second series of ground-vibrations tests and for which complete data were not recorded. No unstable vibrations were observed.

Following the aforementioned tests, the fuselage was rolled 6° and tethered in the rolled position to check the possibility of resonance

conditions resulting from steady forces such as gravity acting in the plane of the rotor. With the model parameters as stated for the second series of ground-vibrations tests (see table III) and with a blade pitch setting of 10°, the rotor speed was slowly increased from zero to 260 rpm. The tethering cables were attached to the upper bay of the fuselage and used to keep the model wheels in contact with the floor. No unstable vibrations were observed.

Three-per-Revolution Rotor-Blade Unsymmetric-Bending Oscillations

During all the flutter runs where the rotor speed exceeded 250 rpm, a very definite three-per-revolution oscillation occurred. The occurrence of this oscillation had not been contemplated, but is believed of general interest and is therefore given. The oscillation involved antisymmetric bending of the blades and appeared as a stable-beat phenomena. The signal from the oscillation was easily identified on the oscillograph records (see, for example, the bending of blades 1 and 2 in fig. 17), but visual attempts to observe the oscillations with the aid of stroboscopic lighting were unsuccessful. Since the oscillograph records for the second series of flutter tests covered a wide range of operating conditions, they were analyzed for the three-per-revolution oscillation data which are presented in table VI. To give an idea of the relative amplitude of the oscillations as a function of blade pitch and rotor speed, the maximum response was arbitrarily assigned unit amplitude and the relative amplitude determined for all other responses. There was some question as to whether this oscillation would exist if the model restraints (tethering cables) were removed. Subsequent tests showed that the oscillation existed in approximately the same proportions whether the model was free or restrained. The oscillation was recorded both while the model was tending to hover and while hovering. Although the source of the oscillations is not definitely known, it is believed that the amplitudes are magnified because the oscillations occur within a range of rotational frequencies which are approximately equal to the natural frequencies of the blades in second bending while rotating.

CONCLUSIONS

Based on the results of an investigation of the flutter and ground vibrations of a $\frac{1}{10}$-scale dynamic model of the XH-17 helicopter, the following conclusions regarding the flutter and ground-vibrations characteristics of the model are made:

1. With the model fuselage rigidly attached to the floor and the relative motion between the pylon and fuselage eliminated, rotor-blade flutter of the classical bending-torsion type occurred in the cyclic

mode at a rotor speed of 369 rpm. The first natural torsional frequencies of the blade at zero rpm were 14.0 cycles per second in the cyclic mode and 20.0 cycles per second in the collective mode. These values correspond to a full-scale tip speed of 789 feet per second and to full-scale frequencies of 27.65 radians per second and 39.5 radians per second, respectively.

2. The flutter speed was raised by increasing the cyclic torsional frequency of the blades. This increase was accomplished by increasing the stiffness of the blade-pitch control mechanism.

3. The flutter speed was also raised by placing weights in the outboard counterweight box located at $\frac{r}{R} = 0.85$ ahead of the blade leading edge.

4. With the model completely assembled and free to vibrate in all of its degrees of freedom, and with the blade mass distribution adjusted to the design value, rotor blade flutter of the classical bending-torsion type occurred as follows:

a. When the blade torsional frequencies were adjusted to 17.4 cycles per second in the cyclic mode and 19.2 cycles per second in the collective mode and the rotor speed was gradually increased without externally vibrating the model, flutter occurred in the collective mode at a rotor speed of 371 rpm. The blade frequencies correspond to full-scale values of 34.4 radians per second and 37.9 radians per second, respectively. The flutter speed corresponds to a full-scale tip speed of 794 feet per second.

b. With the blade frequencies adjusted as in item (a) of this section, the model was shaken vigorously as the rotor speed was increased. Flutter was obtained at a rotor speed of 375 rpm. In this case, the flutter occurred in the cyclic mode. The flutter speed corresponds to a full-scale tip speed of 805 feet per second.

5. With the model rotor mounted on a rigid pylon at a height of 52 inches above the floor, the design counterweights appeared to be more effective in preventing divergence than they were in preventing flutter.

6. No unstable ground vibrations were observed during any of the model tests. These tests included departures from the design configuration both in the direction which would more likely produce unstable ground vibrations and in the direction which would tend to eliminate such vibrations.

Langley Aeronautical Laboratory
National Advisory Committee for Aeronautics
Langley Field, Va.

REFERENCES

1. Theodorsen, Theodore: General Theory of Aerodynamic Instability and the Mechanism of Flutter. NACA Rep. 496, 1935.

2. Theodorsen, Theodore, and Garrick, I. E.: Mechanism of Flutter - A Theoretical and Experimental Investigation of the Flutter Problem. NACA Rep. 685, 1940.

3. Coleman, Robert P.: A Preliminary Theoretical Study of Helicopter-Blade Flutter Involving Dependence upon Coning Angle and Pitch Setting. NACA MR L6G12, 1946.

4. Coleman, Robert P., and Stempin, Carl W.: A Preliminary Theoretical Study of Aerodynamic Instability of a Two-Blade Helicopter Rotor. NACA RM L6H23, 1947.

5. Coleman, Robert P.: Theory of Self-Excited Mechanical Oscillations of Hinged Rotor Blades. NACA ARR 3G29, 1943.

6. Feingold, Arnold M.: Theory of Mechanical Oscillations of Rotors with Two Hinged Blades. NACA ARR 3I13,. 1943.

7. Coleman, Robert P., and Feingold, Arnold M.: Theory of Ground Vibrations of a Two-Blade Helicopter Rotor on Anisotropic Flexible Supports. NACA TN 1184, 1947.

TABLE I.- MODEL AND FULL-SCALE SPANWISE

DISTRIBUTION OF κ

Range of $\frac{r}{R}$	$\kappa = \frac{\pi b^2 \rho}{M}$ (1)	
	Model	Full scale
0.3 to 0.4	0.0308	0.0410
.4 to .5	.0483	.0415
.5 to .6	.0483	.0523
.6 to .7	.0508	.0490
.7 to .8	.0523	.0460
.8 to .9	.0288	.0288
.9 to 1.0	.0323	.0408
Average	0.0428	0.0418

[1] κ is defined as the ratio of a mass of air of a diameter equal to the blade chord to the mass of the blade, both taken for equal lengths along the span.

TABLE II.- MODEL AND FULL-SCALE BLADE FREQUENCIES

FOR THE FLUTTER TESTS

[Model values converted to corresponding full-scale values by frequency scale factor, $1/\sqrt{10}$]

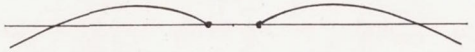
Mode of blade vibration	Frequency (radians/sec) (1)											
	First series				Second series				Third series			
	Model		Full scale		Model		Full scale		Model		Full scale	
	On stops	Off stops	On stops	Off stops	On stops	Off stops	On stops	Off stops	On stops	Off stops	On stops	Off stops
[2]Second bending, antisymmetric	16.6	----	----	----	16.9	----	----	----	19.2	16.5	18.3	----
[3]Second bending, symmetric	23.1	17.0	----	13.2	22.7	17.0	20.8	----	24.3	17.7	20.7	----
[4]Third bending, antisymmetric	----	----	----	----	48.2	----	----	----	50.2	50.0	----	----
[5]Third bending, symmetric	----	----	----	43.4	58.1	----	----	----	60.0	58.1	----	----
First torsion, cyclic	29.4	27.9	----	31.6	44.2	44.4	47.7	----	40.0	34.6	----	34.6
First torsion, collective	51.3	39.9	----	52.5	47.2	46.8	59.7	----	46.2	38.2	----	38.6

[1]The frequencies were measured at zero rotor speed with the blade weight distribution as given in figure 1 (design condition). The torsional frequencies include the effect of blade pitch control stiffness.

[2]Second bending, antisymmetric



[3]Second bending, symmetric



[4]Third bending, antisymmetric



[5]Third bending, symmetric

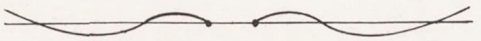


TABLE III.- MODEL AND FULL-SCALE PARAMETERS

FOR THE GROUND-VIBRATIONS TESTS

[Model values are presented in terms of full-scale values]

Parameter	Scale factor	First series		Second series	
		Model	Full scale	Model	Full scale
Gross weight, lb	10^3	41,800	34,800	55,510	52,200
Fuselage weight, lb	10^3	23,730	21,826	37,690	39,226
Suspended weight, lb	10^3	18,080	12,974	17,820	12,974
Fuselage moment of inertia, rolling, slug-ft^2	10^5	30,500	29,800	43,200	41,100
Fuselage moment of inertia, pitching, slug-ft^2	10^5	43,200	37,600	55,400	63,500
Fuselage center-of-gravity location, below rotor plane, in.	10	137	141	165	169
Damping constants, lb-sec/ft	$10^2\sqrt{10}$				
Wheel-strut assembly, front		442	600	253	------
Wheel-strut assembly, rear		544	518	506	------
Pylon (Model values are minimum values from fig. 16.)		900	756	727	756
Effective spring constants, lb/in.	10^2				
Wheel-strut assembly, front		1,610	1,610	2,500	2,085
Wheel-strut assembly, rear		3,080	3,050	5,000	3,980
Pylon at zero thrust		3,100; 6,100	3,076	4,600	6,100
[1]Rotor blade frequencies, radians/sec	$1/\sqrt{10}$				
Second bending, antisymmetric		16.9	------	15.1	------
Second bending, symmetric		22.7	20.8	22.3	20.8
Third bending, antisymmetric		48.2	------	58.0	------
Third bending, symmetric		58.0	------	64.0	------
First torsion, cyclic		44.2	47.8	47.2	47.8
First torsion, collective		47.2	59.7	48.4	59.7
First chordwise bending		16.3	15.9	14.8	15.9
Frequencies of fuselage motion, model blade replaced by an equivalent mass at rotor hub flange, radians/sec	$1/\sqrt{10}$				
Pitching, brakes on:					
First mode		----------	3.73	4.06	------
Second mode		----------	13.82	16.40	------
Third mode		----------	22.97	27.70	------
Pitching, brakes off:					
First mode		----------	7.95	5.28	------
Second mode		----------	19.34	17.30	------
Third mode		----------	------	32.40	------
Rolling:					
First mode		----------	4.00	3.63	------
Second mode		----------	15.47	16.20	------
Third mode		----------	31.74	37.20	------
Pitching, hovering:					
First mode		----------	------	2.90	4.27
Rolling, hovering:					
First mode		----------	------	3.98	4.51

[1]The rotor-blade frequencies were measured with the blades resting on the stops at zero rotor speed. The torsional frequencies include the effect of the blade-pitch control stiffness.

NACA

TABLE IV.- SUMMARY OF MODEL FLUTTER TEST DATA

[Model speeds and frequencies may be converted to full-scale values with the aid of fig. 14]

Flutter test number	Blade pitch angle (deg)	Rotor top speed (rpm)	Flutter speed (rpm)	Duration of flutter (sec)	Rotor speed at end of flutter (rpm)	Flutter mode (blade bending)	Flutter mode (blade torsion)	Flutter frequency (cps)	Inboard counterweight (attached or removed)	Additional weight located in outboard counterweight box (lb)	Location of additional weight ahead of blade quarter-chord line (in.)
First series of flutter tests											
1	0	369	369	2	279	Antisymmetric	Cyclic	11.45	Attached	0	----
2	0	382	← No flutter obtained →						Attached	.046	4.01
3	0	371	371	2.3	286	Antisymmetric	Cyclic	11.05	Attached	.046	2.37
4	5	382	← No flutter obtained →						Attached	.046	5.59
Second series of flutter tests											
1	0	375	No flutter obtained						Attached	0.046	5.59
2	0	377							Attached	0	----
3	0	369							Removed	0	----
4	5	366							Attached	.046	5.59
5	5	356							Attached	0	----
6	5	345							Removed	0	----
7	8	305							Removed	0	----
8	10	276							Attached	.046	5.59
9	10	291							Attached	0	----
10	10	287							Removed	0	----
11	15	251							Attached	.046	5.59
12	15	253							Attached	0	----
13	15	251							Removed	0	----
Third series of flutter tests											
1	0.5	371	371	2	313	Symmetric	Collective	15.60	Attached	0	----
2	.5	387	387	1.3	319	Symmetric	Collective	15.72	Attached	0	----
3	.5	387	387	1.7	313	Symmetric	Collective	15.72	Attached	0	----
4	.5	379	379	2.7	327	Antisymmetric	Cyclic	12.88	Attached	0	----
5	.5	375	375	1.5	367	Antisymmetric	Cyclic	13.04	Attached	0	----
6	.5	377	377	1.7	367	Antisymmetric	Cyclic	13.01	Attached	0	----

TABLE V.- EFFECT OF COUNTERWEIGHTS ON MODEL ROTOR FLUTTER

(Rotor mounted on rigid pylon)

Flutter test number	Blade pitch angle (deg)	Flutter speed (rpm)	Flutter mode (blade bending)	Flutter mode (blade torsion)	Flutter frequency (cps)	Inboard counterweight (attached or removed)	Outboard counterweight (attached or removed)	Remarks
1	0.5	392	Antisymmetric	Cyclic	13.8	Attached	Attached	No divergence visible before flutter
2	.5	391	Antisymmetric	Cyclic	13.8	Removed	Attached	Very little divergence before flutter
3	.5	383	Antisymmetric	Cyclic	13.8	Attached	Removed	Considerable divergence before flutter
4	.5	379	Antisymmetric	Cyclic	13.9	Removed	Removed	Divergence so pronounced that only mild flutter obtained

TABLE VI.- TABULATION OF DATA ON 3-PER-REVOLUTION ROTOR

BLADE ANTISYMMETRIC BENDING OSCILLATIONS

Blade pitch angle (deg)	[1]Rotor speed at which 3-per-revolution oscillation occurred (rpm)	Frequency of 3-per-revolution oscillation (cps)	Relative amplitude	Approximate beat period (sec)
[2]With 0.046-pound additional weight located in the outboard counterweight box, 5.59 inches ahead of the blade quarter chord.				
0	266 (min)	13.30	0.29	---
	375 (max)	18.80	.34	---
5	242 (min)	12.10	.37	3.7
	366 (max)	18.30	.89	---
10	233 (min)	11.65	.43	---
	276 (max)	13.80	.86	3.3
15	250 (min)	12.50	.54	---
	251 (max)	12.55	.54	---
With zero additional weight located in the outboard counterweight box (design condition).				
0	260 (min)	13.00	0.31	5.4
	377 (max)	18.90	.37	2.2
5	271 (min)	13.50	.51	3.5
	356 (max)	17.80	.97	3.3
10	232 (min)	11.60	.46	---
	291 (max)	14.55	.57	2.5
15	250 (min)	12.50	.72	---
	253 (max)	12.65	.72	---
With zero additional weight in the outboard counterweight box and with the inboard counterweight completely removed.				
0	269 (min)	12.95	0.17	5.5
	369 (max)	18.45	.26	---
5	238 (min)	11.90	.29	5.5
	345 (max)	17.25	1.00	1.6
10	226 (min)	11.30	0.26	---
	287 (max)	14.35	.80	2.0
15	250 (min)	12.50	.48	---
	251 (max)	12.55	.48	---

[1]The maximum value was the maximum rotor speed obtained on the model during the run.

[2]The design blade weight distribution is given in figure 1.

NACA

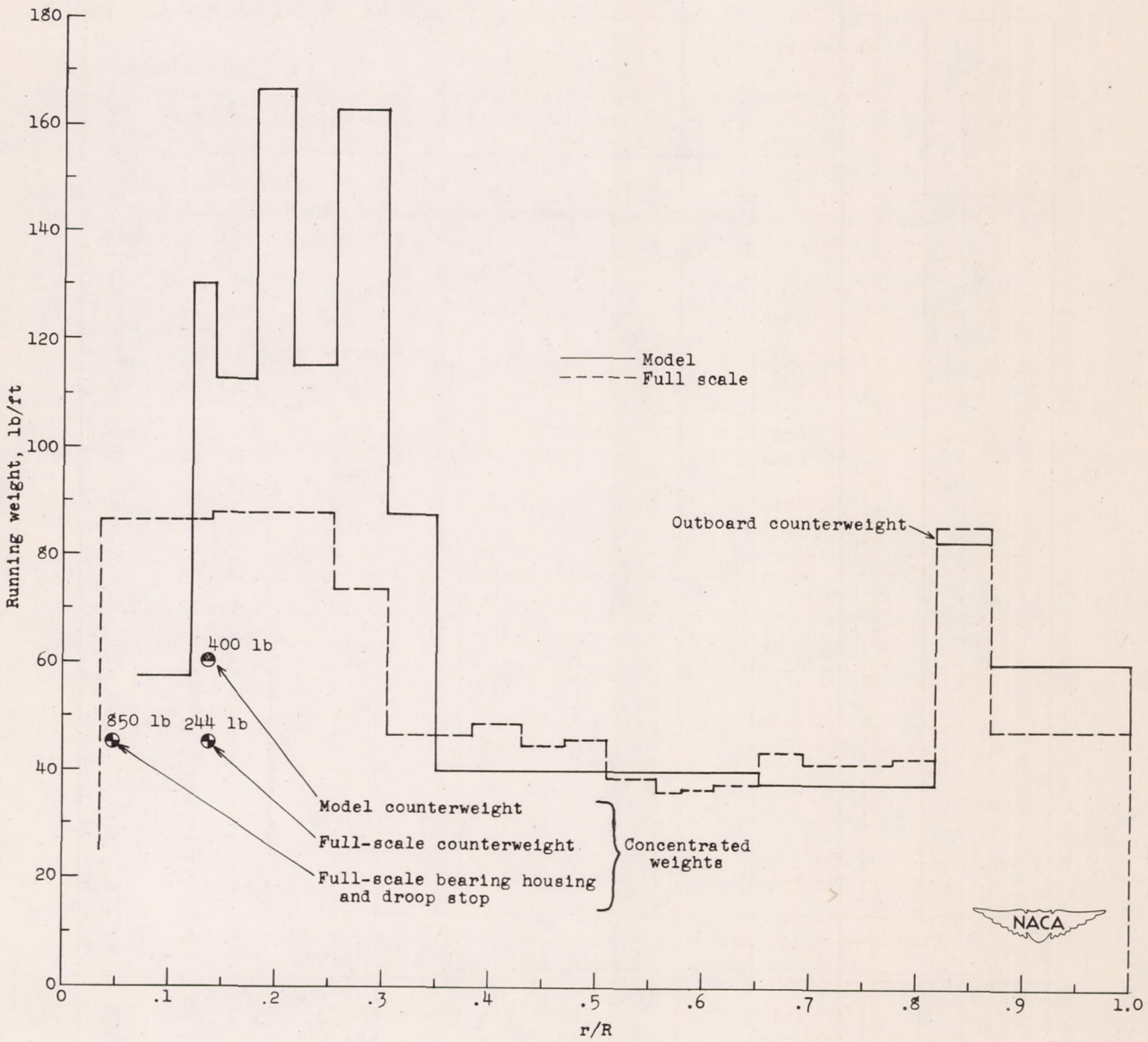


Figure 1.- Model and full-scale spanwise mass distribution, model values multiplied by scale factor of 100.

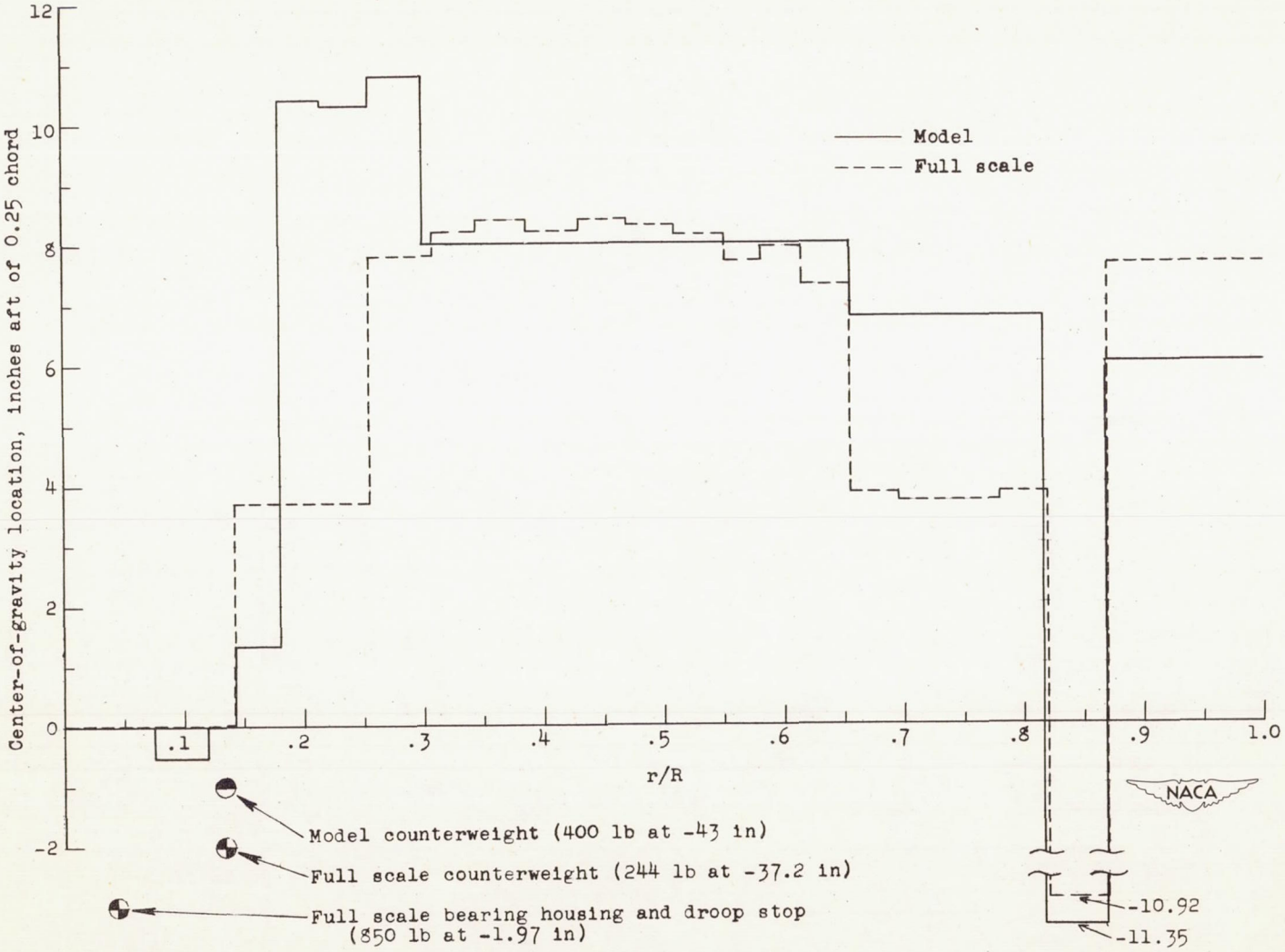


Figure 2.- Model and full-scale chordwise center-of-gravity location, model values multiplied by scale factor of 10.

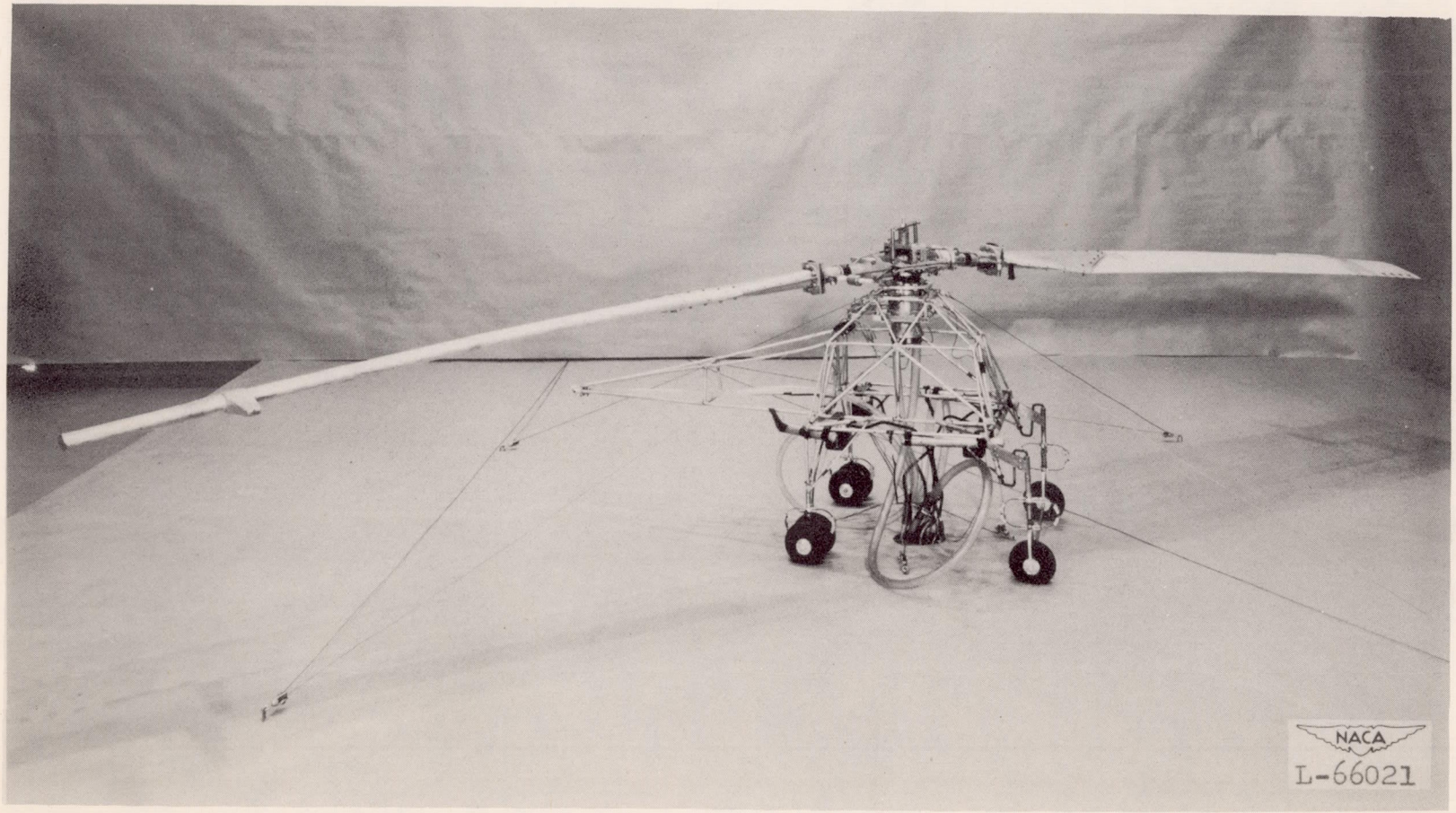


Figure 3.- Model in preparation for ground-vibrations tests.

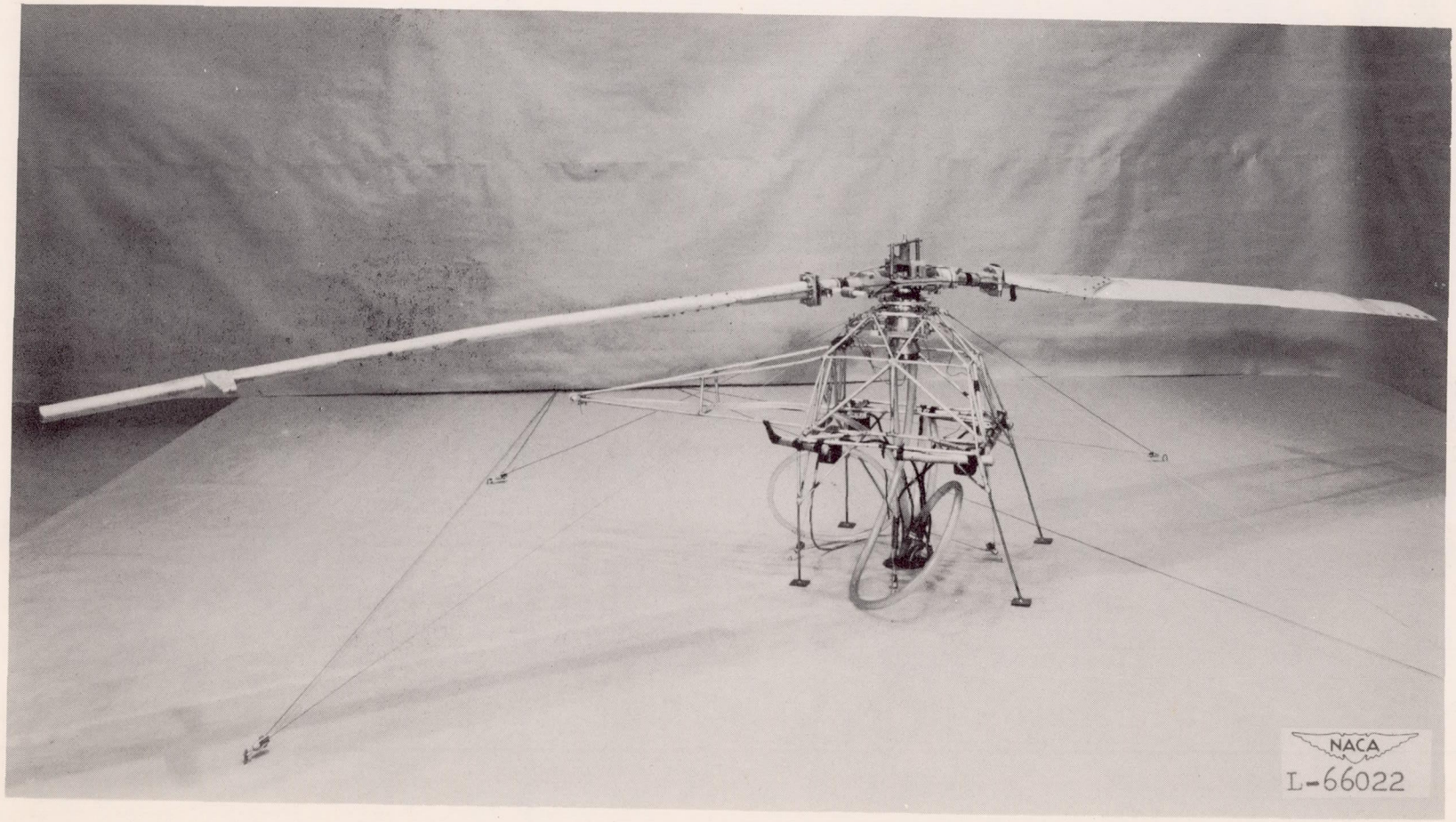


Figure 4.- Model with wheel-strut assemblies replaced by flanged supports in preparation for the first series of flutter tests.

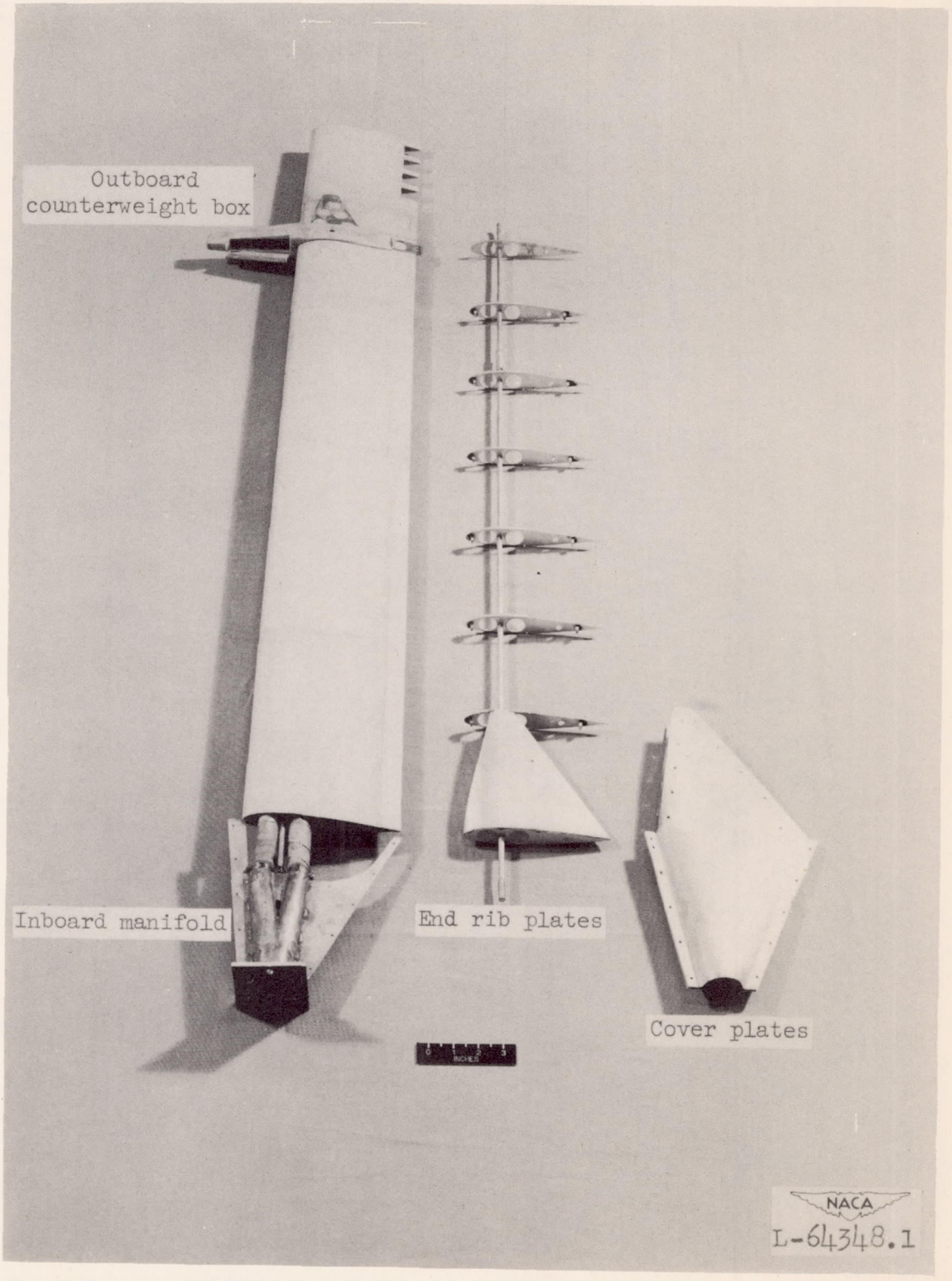


Figure 5.- Rotor-blade assembly.

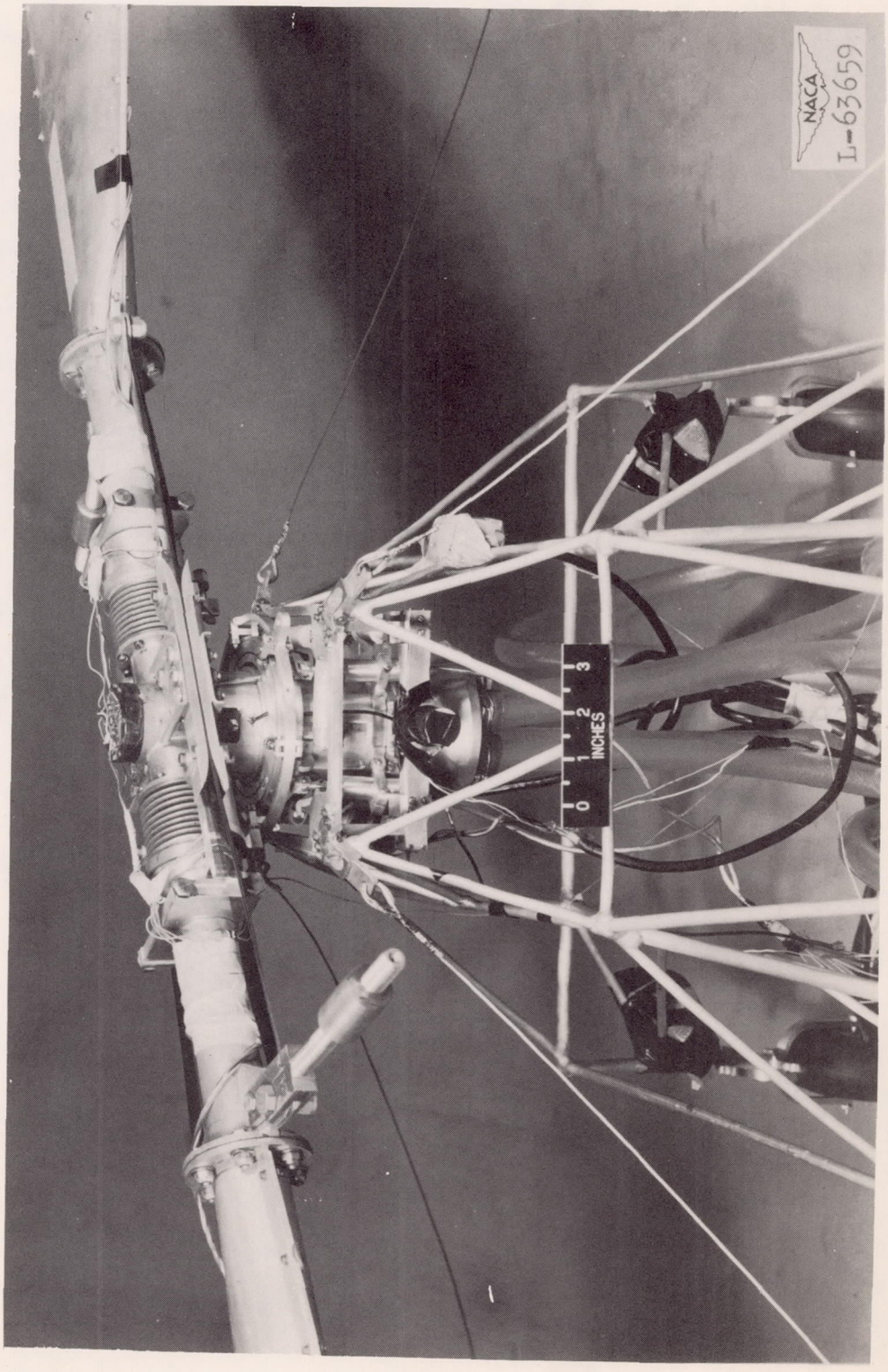


Figure 6.- Rotor-hub, pylon, and fuselage assembly.

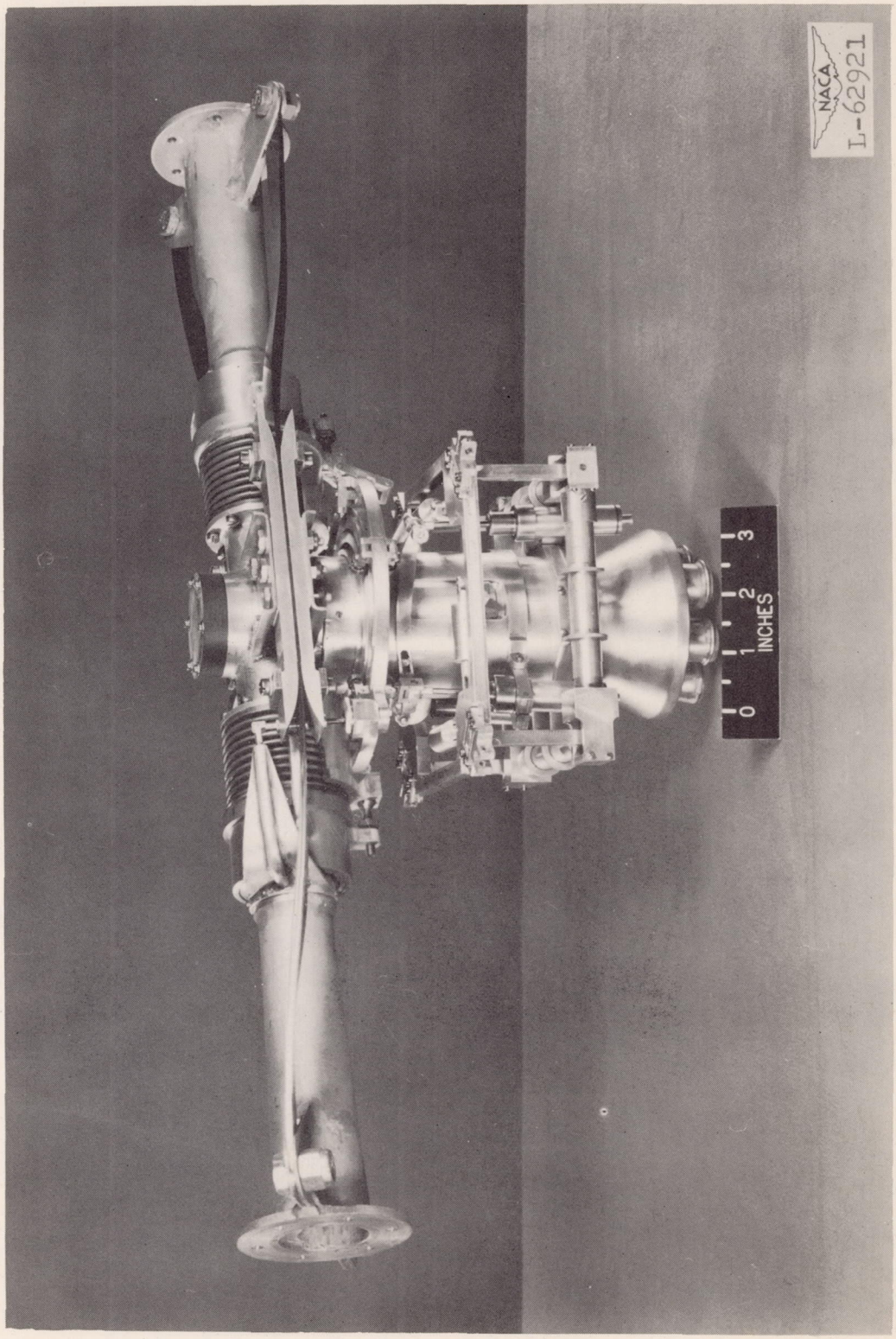


Figure 7.- Rotor-hub and pylon assembly.

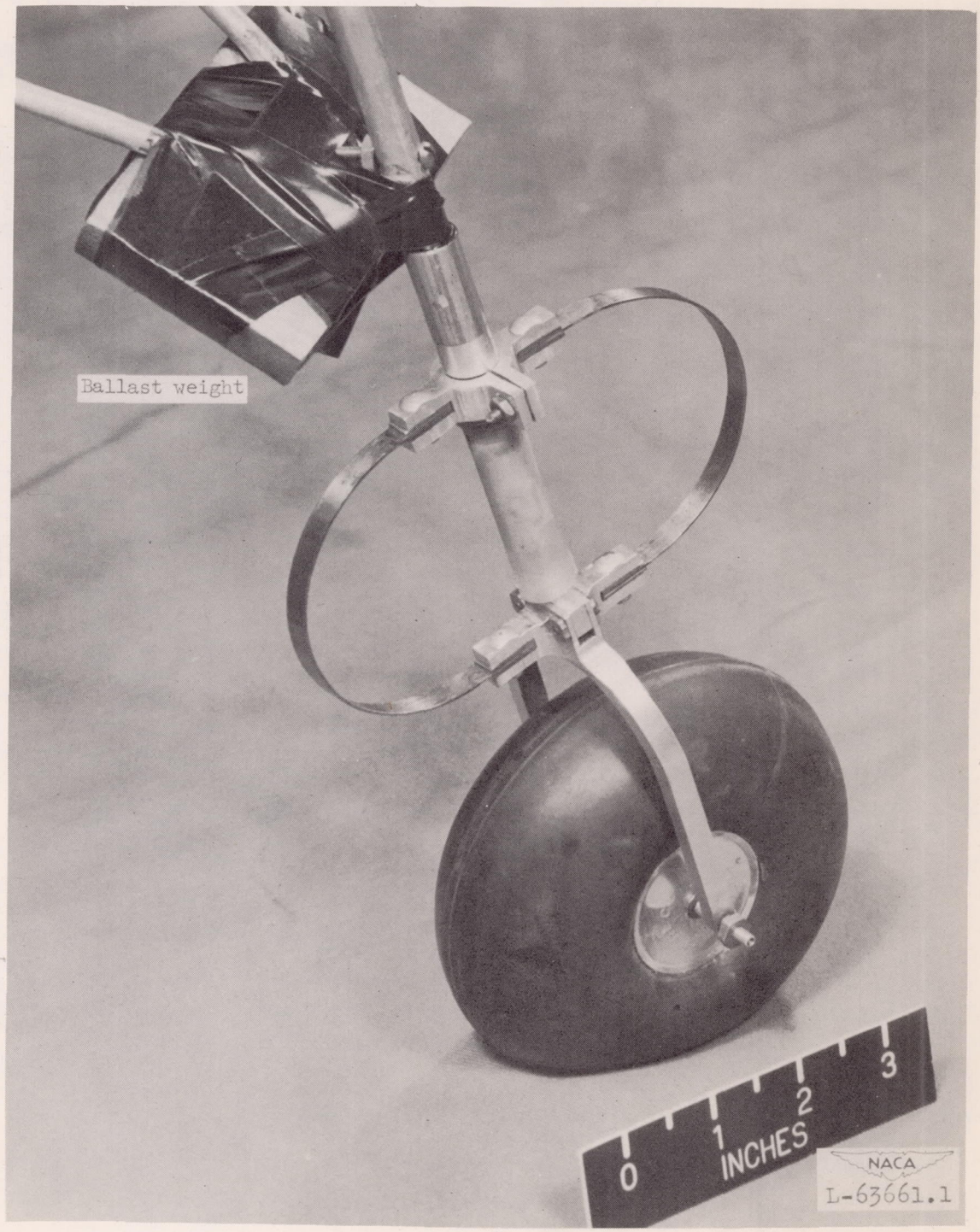


Figure 8.- Wheel-strut assembly, front.

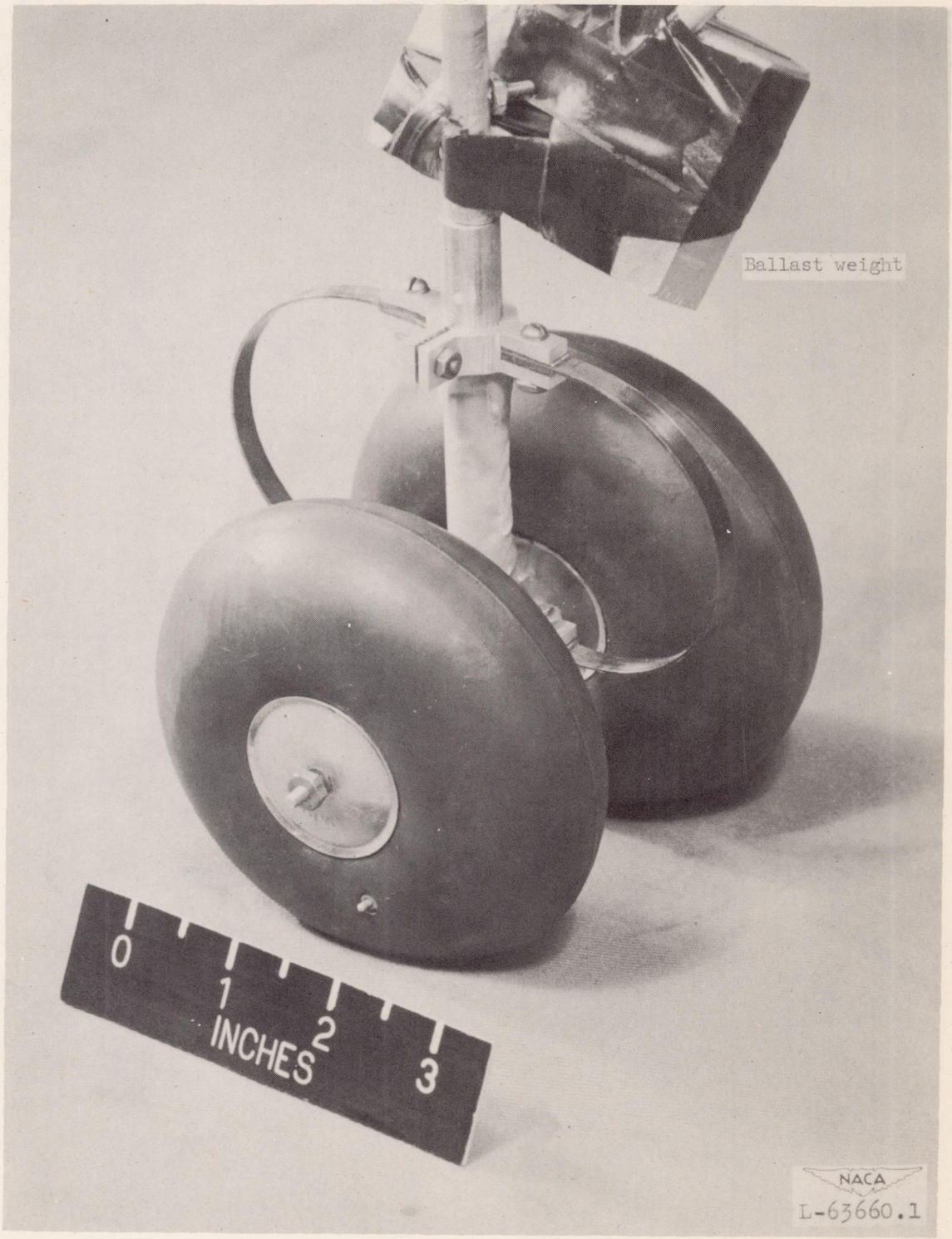


Figure 9.- Wheel-strut assembly, rear.

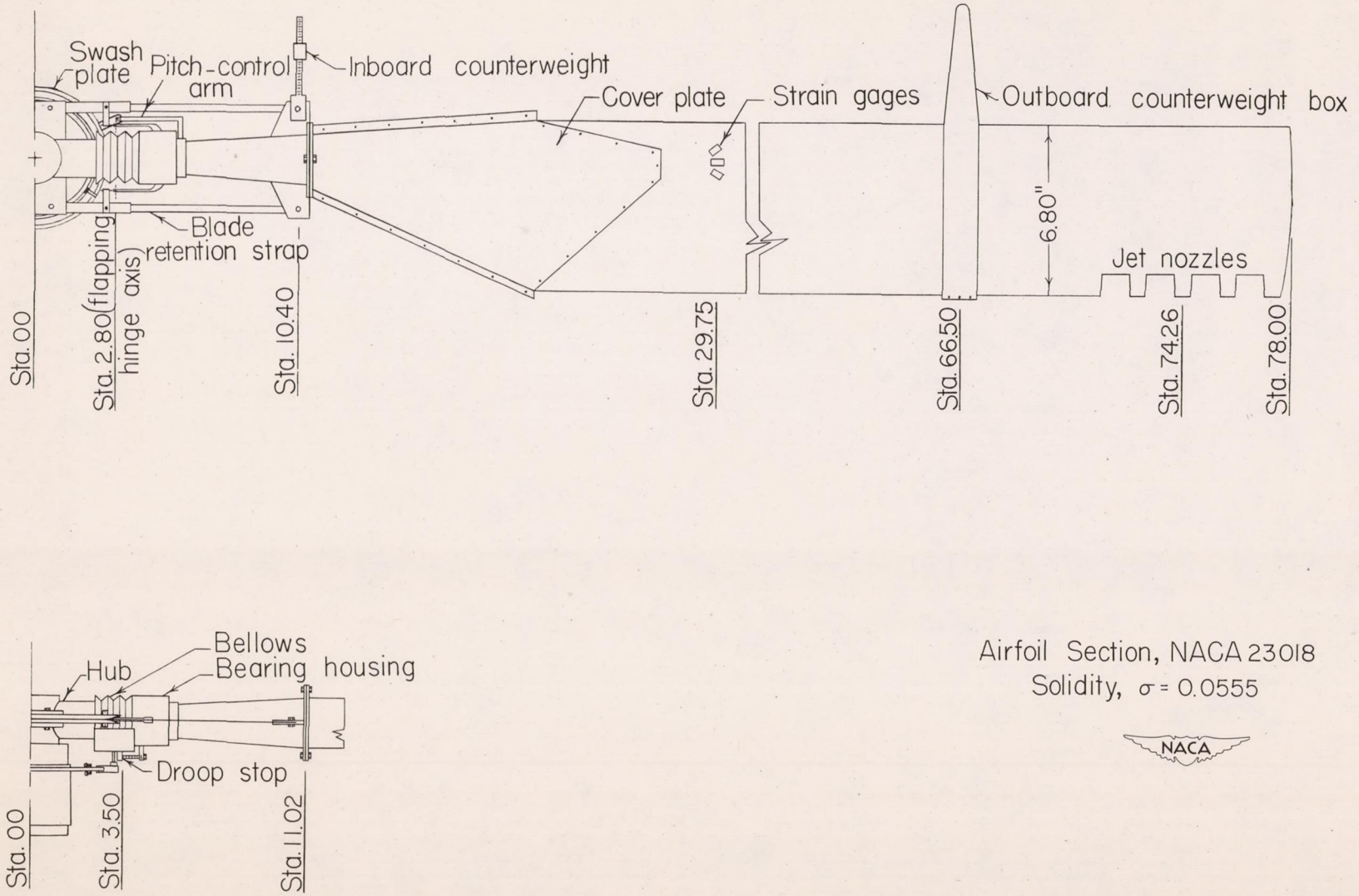


Figure 10.- Detail sketch of rotor assembly.

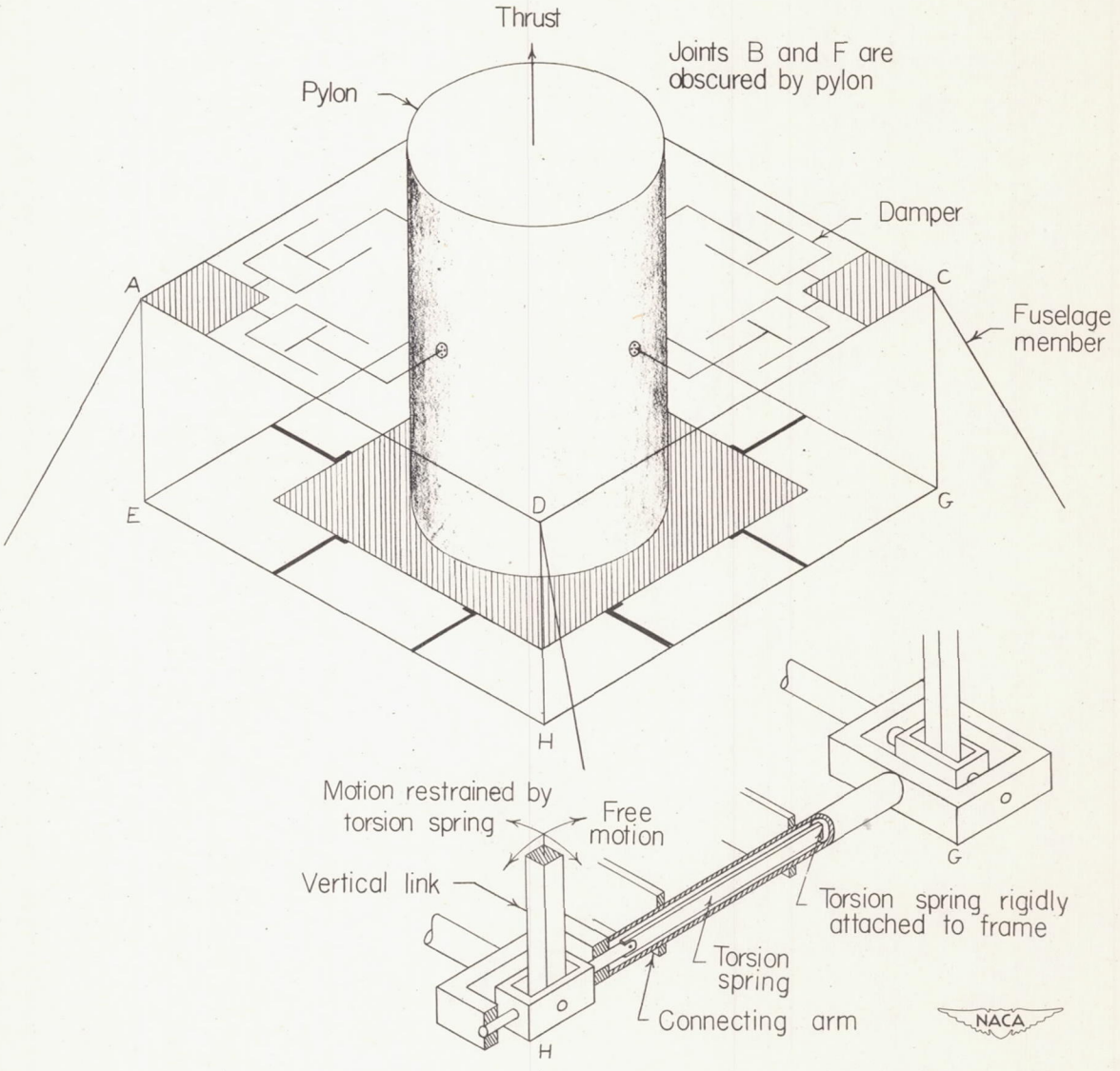


Figure 11.- Schematic diagram of rotor-suspension system and detail of one torsion-spring assembly.

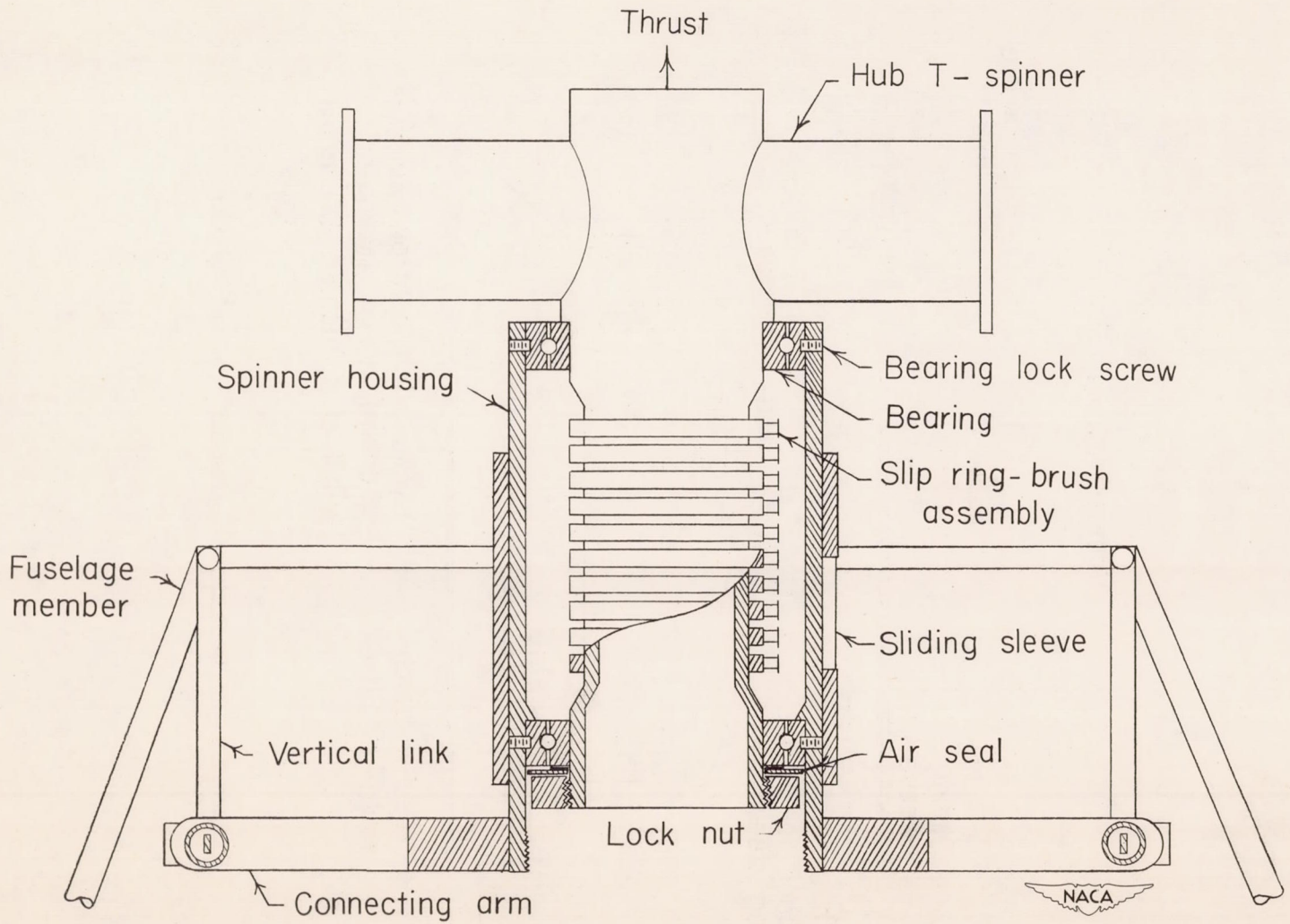


Figure 12.- Schematic diagram of pylon.

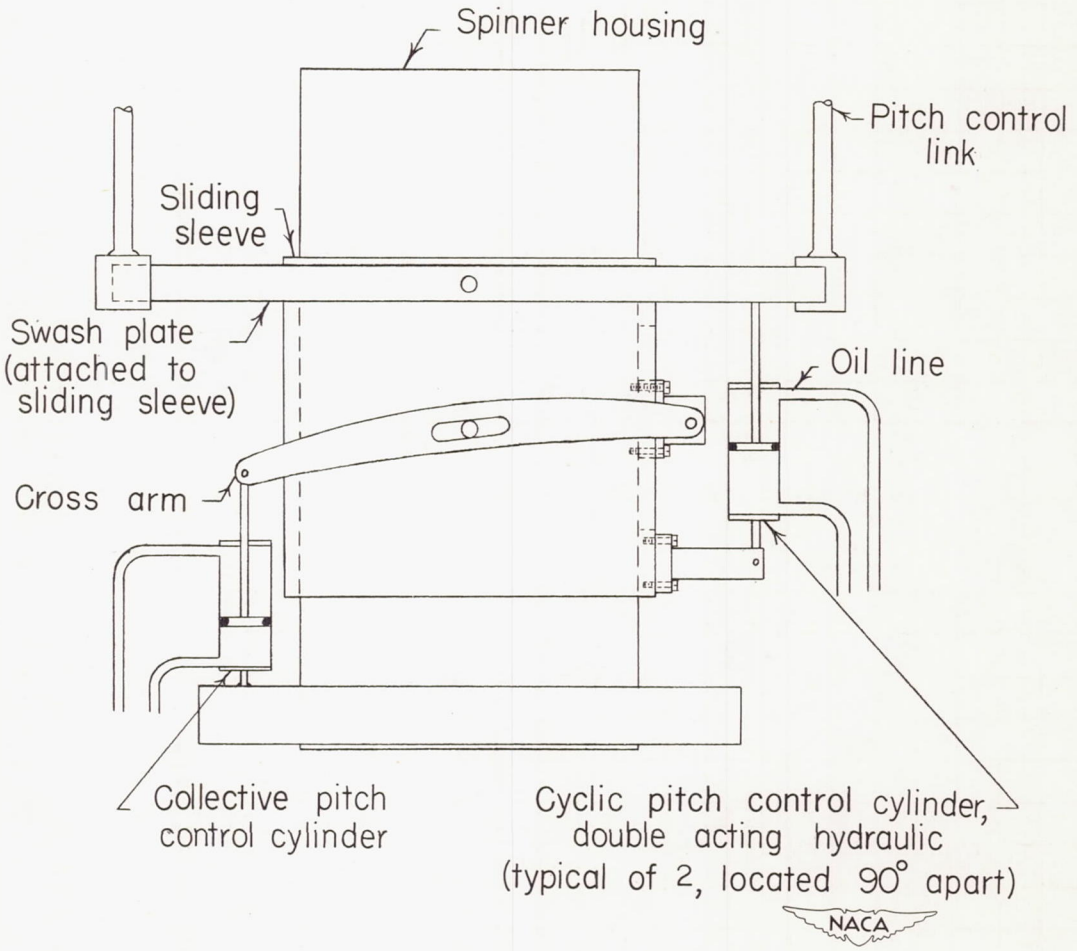
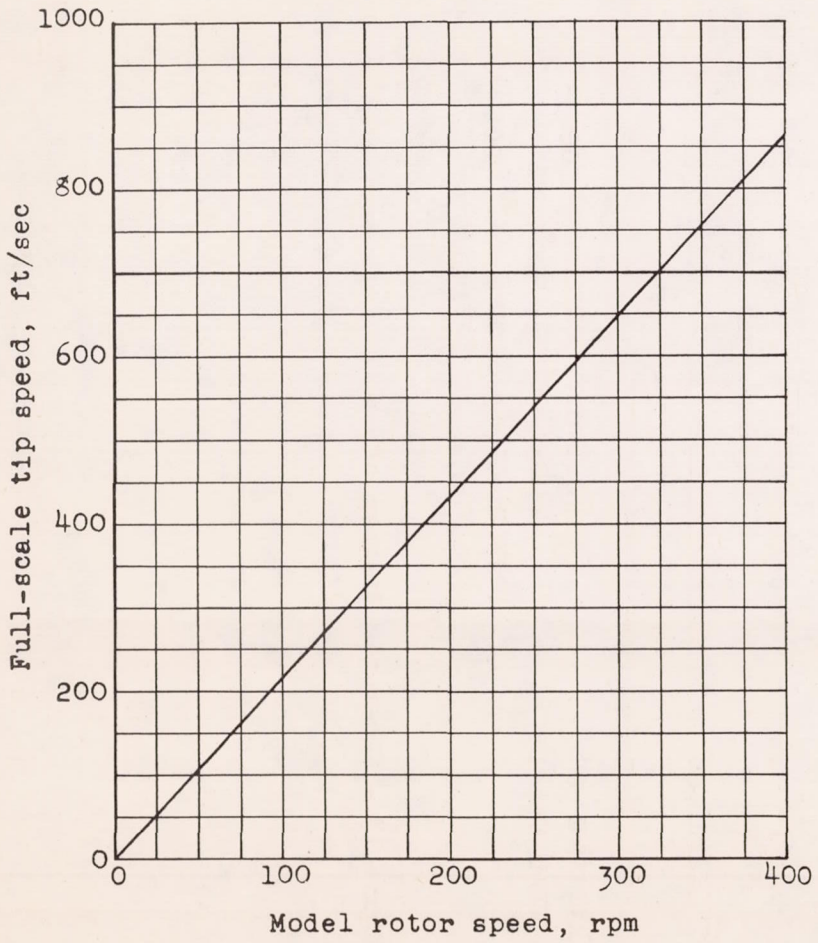
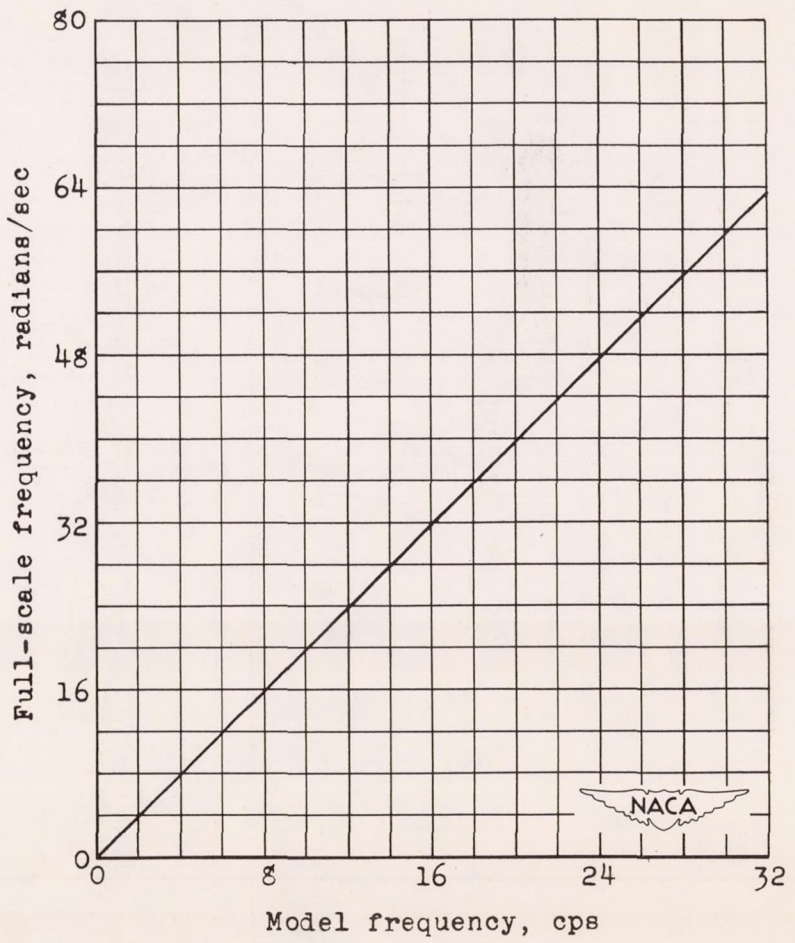


Figure 13.- Schematic diagram of control system.



(a) Rotor speeds.



(b) Frequencies.

Figure 14.- Chart for converting model rotor speeds and frequencies to full-scale tip speeds and frequencies.

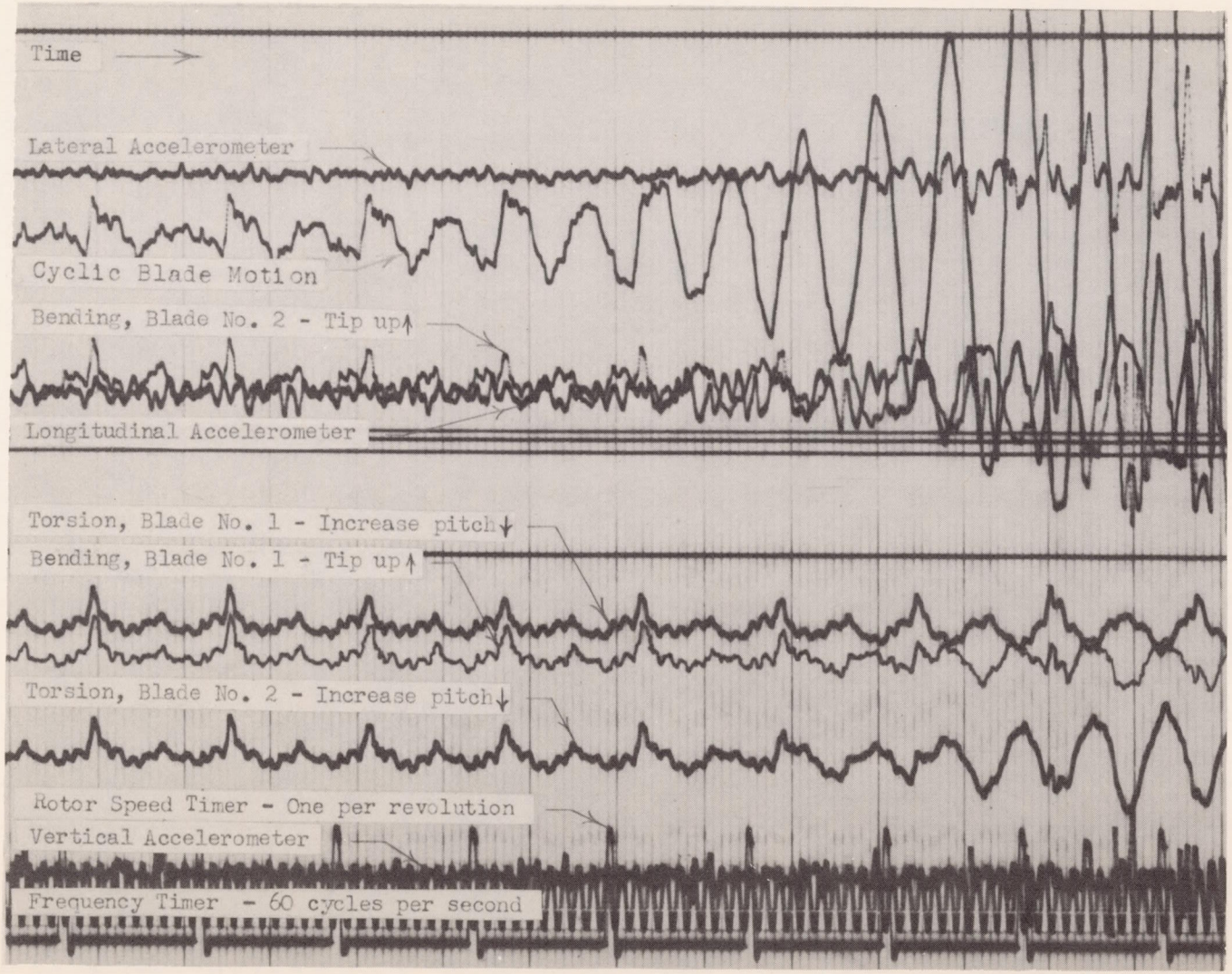


Figure 15.- Portion of oscillograph record showing rotor-blade flutter.

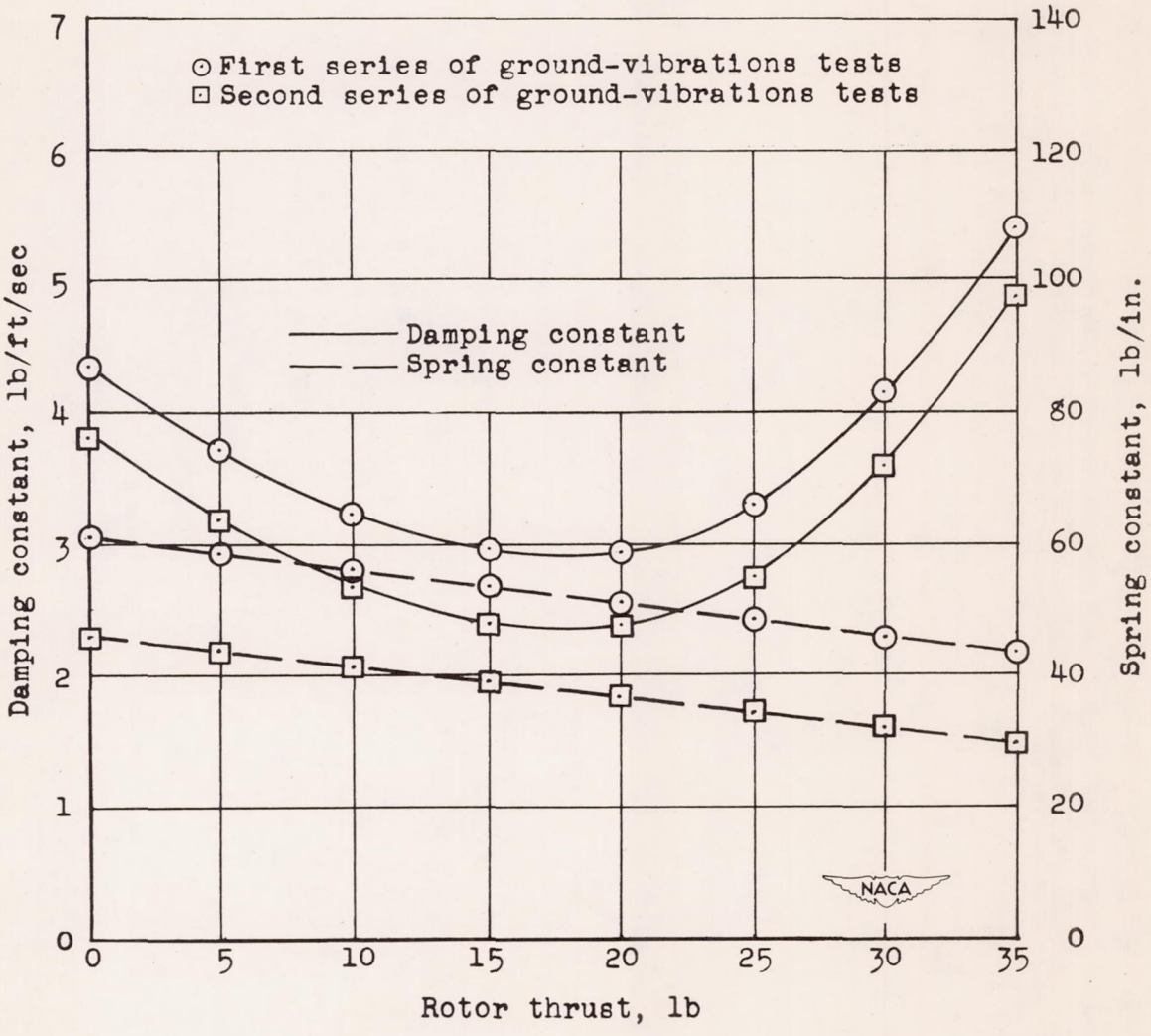


Figure 16.- Effective model pylon spring and damping constants.

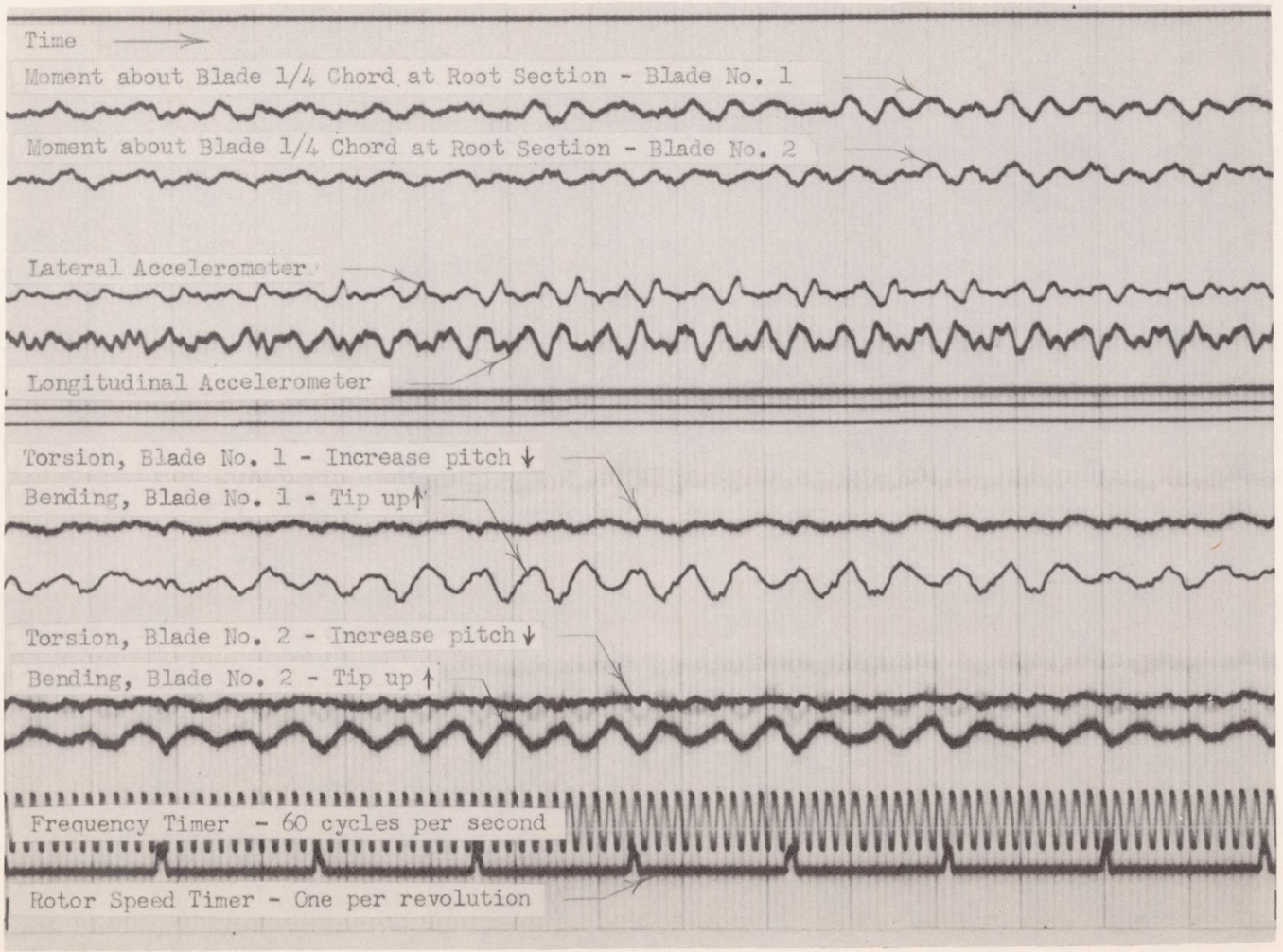


Figure 17.- Portion of oscillograph record showing three-per-revolution rotor-blade antisymmetric bending oscillation.

NACA - Langley Field, Va.